Check for updates

Peptide-mediated liquid–liquid phase separation and biomolecular condensates†

Guangle Li,[a] Chengqian Yuan*[a] and Xuehai Yan ⓘD *[abc]

Liquid–liquid phase separation (LLPS) is a cornerstone of cellular organization, driving the formation of biomolecular condensates that regulate diverse biological processes and inspire innovative applications. This review explores the molecular mechanisms underlying peptide-mediated LLPS, emphasizing the roles of intermolecular interactions such as hydrophobic effects, electrostatic interactions, and π–π stacking in phase separation. The influence of environmental factors, such as pH, temperature, ionic strength, and molecular crowding on the stability and dynamics of peptide coacervates is examined, highlighting their tunable properties. Additionally, the unique physicochemical properties of peptide coacervates, including their viscoelastic behavior, interfacial dynamics, and stimuli-responsiveness, are discussed in the context of their biological relevance and engineering potential. Peptide coacervates are emerging as versatile platforms in biotechnology and medicine, particularly in drug delivery, tissue engineering, and synthetic biology. By integrating fundamental insights with practical applications, this review underscores the potential of peptide-mediated LLPS as a transformative tool for advancing science and healthcare.

1. Introduction

1.1. Definition and significance of liquid–liquid phase separation (LLPS)

Liquid–liquid phase separation (LLPS) is a fundamental physicochemical process in which a homogeneous solution of macromolecules, such as polymers or biomacromolecules, spontaneously separates into two distinct liquid phases: one enriched in these macromolecules and the other depleted of them.[1,2] This process results in the formation of dense, liquid-like droplets suspended within a more dilute surrounding phase. The phase behavior of LLPS can be represented in phase

[a] State Key Laboratory of Biopharmaceutical Preparation and Delivery, Institute of Process Engineering, Chinese Academy of Sciences, Beijing 100190, China.
E-mail: cqyuan@ipe.ac.cn, yanxh@ipe.ac.cn
[b] School of Chemical Engineering, University of Chinese Academy of Sciences, Beijing, 100049, China
[c] Center for Mesoscience, Institute of Process Engineering, Chinese Academy of Sciences, Beijing, 100190, China
† Electronic supplementary information (ESI) available. See DOI: https://doi.org/10.1039/d4sm01477d

Guangle Li received his PhD degree from the Institute of Chemistry, Chinese Academy of Sciences (CAS). He then joined Prof. Yi Zuo's group as a postdoc at the University of Hawaii at Manoa. Currently, he is an associate professor at the Institute of Process Engineering (IPE), CAS. His research interests are focused on liquid–liquid phase separation, biointerfaces, and bioinspired materials.

Guangle Li

Chengqian Yuan received his PhD degree from the Institute of Chemistry, Chinese Academy of Sciences. He then joined Prof. Xuehai Yan's group as a postdoc at the State Key Laboratory of Biopharmaceutical Preparation and Delivery, IPE, CAS. Currently, he is an associate professor at the IPE, CAS. His research interests include peptide self-assembly and engineering, biomolecular condensates and glass, and phase separation.

Chengqian Yuan

diagrams, which map the conditions under which phase separation occurs.[2,3] The study of LLPS in polymers has yielded significant insights into material science, particularly by enabling the design of advanced materials with tunable properties derived from phase-separated structures.[4] More recently, the significance of LLPS in cell biology has been recognized as it offers a novel framework for understanding intracellular organization and compartmentalization.[5–7] Unlike traditional membrane-bound organelles, LLPS-driven self-assembly generates distinct cytoplasmic and nucleoplasmic compartments, forming biomolecular condensates, some of which evolve into functionally specialized membraneless organelles.[8,9] These condensates exhibit dynamic, liquid-like properties, such as rapid component exchange, fusion, and reformation, which are essential for numerous cellular functions.[10–12] Membraneless organelles formed through LLPS are involved in a broad range of physiological functions, such as the formation of heterochromatin, storage of nucleic acids, regulating gene expression, stress response, and signal transduction.[11,13–17] These structures are critical for maintaining cellular homeostasis and orchestrating molecular transport and cell division.[18–21] The realization that LLPS is a fundamental mechanism underlying the formation of these compartments has revolutionized our understanding of cell biology, prompting a reevaluation of numerous biological processes.

The recognition of LLPS has profound implications for human health, as it has become increasingly clear that this fundamental biological process is intimately linked to the pathogenesis of various diseases.[7,22] Aberrant phase separation has been implicated in a range of conditions, including neurodegenerative disorders, cancer, and infectious diseases.[23–26] In neurodegenerative diseases like Alzheimer's disease and amyotrophic lateral sclerosis (ALS), the dysregulation of LLPS can result in the formation of pathological protein aggregates, often due to the transition of biomolecular condensates from liquid-like to solid-like states, as depicted in Fig. 1.[6,7,27] These aggregates are believed to arise from the inappropriate or irreversible maturation of dynamic biomolecular condensates, ultimately causing cellular dysfunction and neurodegeneration.[28]

Xuehai Yan is a full professor at the Institute of Process Engineering, Chinese Academy of Sciences. Currently, he is the deputy director of the State Key Laboratory of Biopharmaceutical Preparation and Delivery and the Center of Mesoscience, IPE, CAS. His research interests are focused on peptide self-assembly and engineering, supramolecular colloids and crystals, phase evolution and dynamic transition, as well as phototherapy and immunotherapy.

Xuehai Yan

Similarly, in cancer, misregulated LLPS can alter the behavior of condensates involved in gene expression and cell cycle control, contributing to uncontrolled cell proliferation and tumor development.[24] In infectious disease, pathogens may hijack host cells' LLPS mechanisms to enhance their replication or to evade immune detection, further illustrating the broad relevance of LLPS in disease processes.[22,29] The growing body of evidence underscores the importance of LLPS not only as a fundamental mechanism for normal cellular function but also as a critical factor in disease pathogenesis. Understanding the nuances of LLPS dysregulation opens new avenues for therapeutic intervention, as targeting the specific molecular interactions that govern phase separation could provide novel strategies for treating disease associated with aberrant condensate formation.[30] Thus, LLPS represents a promising area of research with significant potential to inform the development of new therapies to restore normal cellular function and to prevent disease progression.

1.2. Protein-mediated LLPS and biomolecular condensates

Protein-mediated LLPS. Biomolecular condensates formed *via* protein-mediated LLPS are important for cellular spatial organization, offering a versatile mechanism independent of membrane-bound compartments. These condensates are built from key molecular components: multivalent proteins or intrinsically disordered regions (IDRs) (Fig. 2A).[31,32] IDRs, in particular, lack a rigid structure and exist as dynamic ensembles of conformations, with their primary sequences dictating their phase separation propensity and physical properties of the resulting condensates, such as viscoelasticity and stability.[2,33] Through weak, transient interactions, including hydrophobic effects, electrostatic interactions, and π–π stacking, IDRs drive the assembly of dense, liquid-like condensates that remain distinct from the surrounding dilute phase. Factors such as sequence composition, interaction motif density and spatial arrangement, and linker properties further tune the phase behavior and material properties of these IDR-driven assemblies, underscoring their flexibility and adaptability in cellular contexts.[34,35]

The concept of scaffold and client proteins is fundamental to understanding the molecular mechanisms that govern the formation, function, and regulation of biomolecular condensates.[37] Scaffold proteins are critical for initiating and maintaining phase separation, acting as the structural backbone of condensates by mediating multivalent interactions through multiple interaction motifs or domains. These interactions drive phase separation and provide a robust network that sustains LLPS. Additionally, scaffold proteins play a key role in recruiting client proteins, which, although unable to phase-separate independently, can be incorporated into pre-existing condensates. Often, these interactions involve RNA, particularly in the formation of RNA/protein-rich membraneless organelles.[38] RNA, especially those with repetitive sequences, enhances the multivalent interactions necessary for LLPS, acting as both structural components and functional regulators within condensates.[11] The architecture of scaffold proteins typically includes either multiple folded domains that interact with short linear motifs
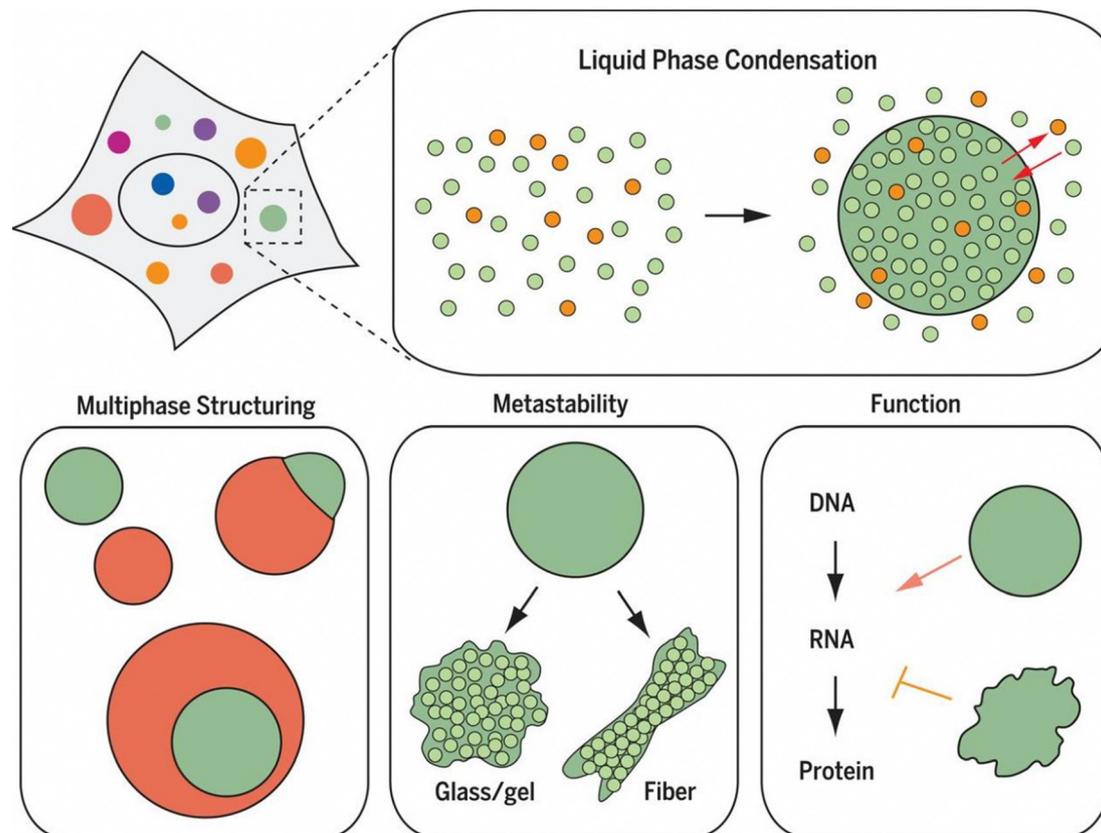
Fig. 1 Liquid–liquid phase separation (LLPS) as a fundamental mechanism of cellular organization. LLPS enables the formation of dynamic biomolecular condensates, or membraneless organelles, that selectively concentrate specific molecules through controlled phase separation. These condensates exhibit diverse behaviors, including multiphase structuring and transitions from liquid-like to solid-like states. Such condensates play significant roles in regulating cellular functions, including RNA transcription and protein translation, by creating specialized microenvironments that facilitate specific biochemical reactions and information flow within the cell. Reprinted with permission.[6] Copyright 2017, The American Association for the Advancement of Science.

in other proteins or IDRs with multiple interacting motifs or "stickers".[35,39] These IDRs mediate weak multivalent interactions essential for driving phase separation. Studies have shown that scaffold valency lowers the saturation concentration required for phase separation, reinforcing their pivotal role in condensate formation.[2]

Examples of biomolecular condensates in biological systems. Biomolecular condensates, formed through LLPS, represent a diverse class of membraneless organelles crucial for cellular organization and function. Spanning a size range from hundreds of nanometers to several micrometers, biomolecular condensates include notable examples such as nucleoli, stress granules, P granules, and Cajal bodies.[6,36,40–44] A pivotal discovery in the study of biomolecular condensates was the observation that P granules in *Caenorhabditis elegans* germ cells exhibit liquid-like behavior (Fig. 2B).[36] Composed of proteins and RNAs, P granules are notably larger (2–4 μm) than many other cellular condensates, making them ideal for quantitative analysis.[5] Their liquid-like properties were first observed in their ability to fuse into spherical shapes, flow and deform under shear forces, and undergo fission. Photobleaching experiments further revealed rapid internal dynamics, with

proteins exchanging between the granule and the cytoplasm within seconds. Subsequent studies extended these findings to other condensates such as nucleoli, stress granules, and Cajal bodies, all of which similarly exhibit liquid-like properties. These discoveries suggest that LLPS is a universal mechanism underpinning the assembly and function of many biomolecular condensates in biological systems. Despite their dynamic nature, biomolecular condensates exhibit remarkable stability in size and shape, often persisting for minutes to hours. This balance between stability and fluidity is achieved through constant molecular exchange with surrounding cytoplasm or nucleoplasm, a process essential for their function. Moreover, condensates are highly responsive to internal and external stimuli, such as thermal or osmotic stress, enabling them to form or dissolve as needed to meet cellular demands.[17,45]

Role in cellular functions and physiology. Biomolecular condensates formed *via* protein-mediated LLPS play a vital role in a wide range of cellular functions and physiological processes.[46] By enabling the compartmentalization and concentration of specific biochemical reactions without membranes, these condensates facilitate spatial organization critical for gene regulation, signal transduction, and stress response.
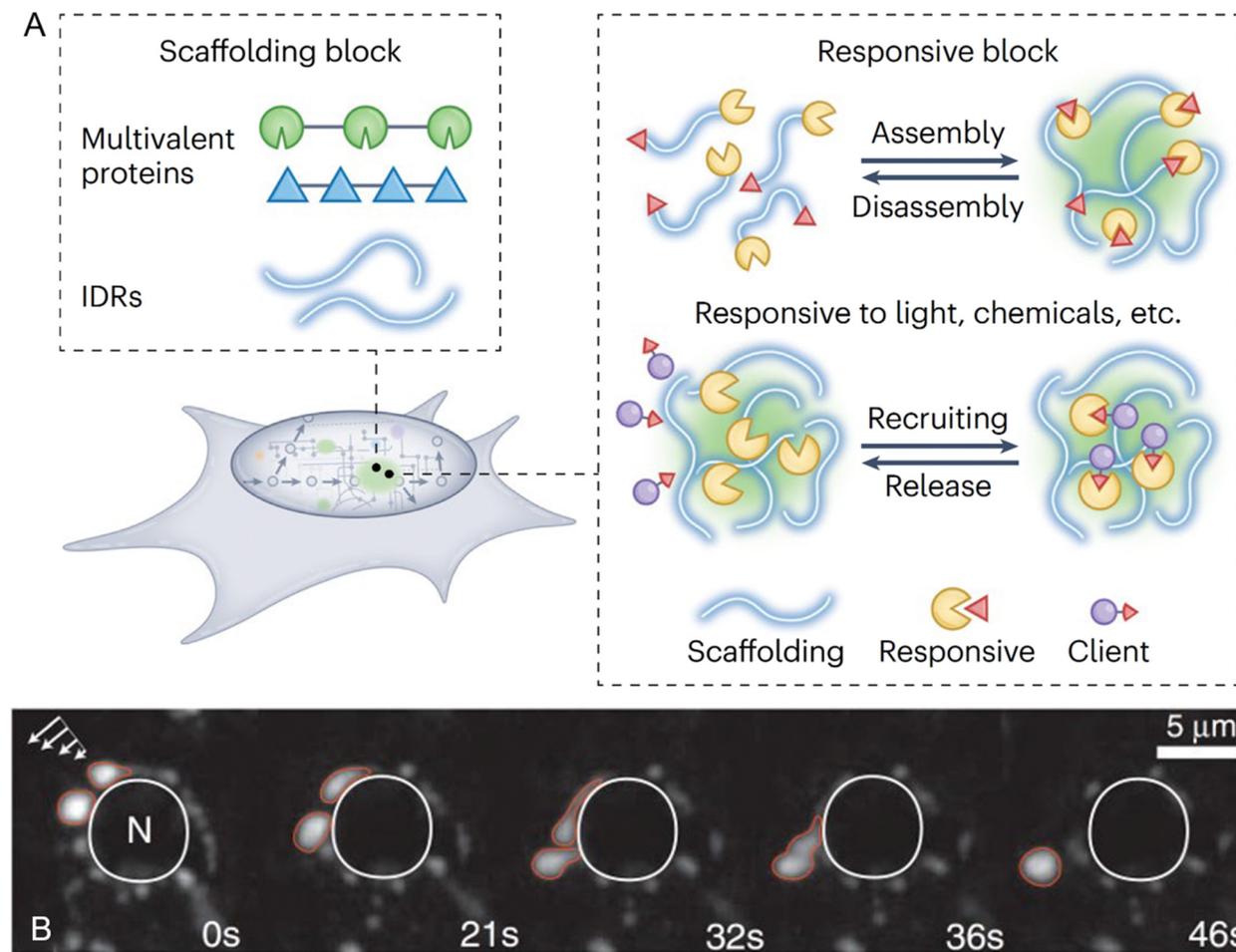
Fig. 2 Protein-mediated liquid–liquid phase separation and biomolecular condensates. (A) Building blocks and functional responsiveness of biomolecular condensates. Multivalent proteins or intrinsically disordered regions (IDRs) act as scaffolds to drive phase separation and condensate formation. These condensates exhibit responsiveness to environmental stimuli, enabling controlled assembly and disassembly as well as the selective recruitment and release of client proteins, highlighting their adaptability to dynamic biological processes. Reprinted with permission.[32] Copyright 2022 Springer Nature. (B) Dynamic liquid-like properties of P granules in *Caenorhabditis elegans* germ cells. Time-lapse imaging demonstrates the deformation, dripping, and fusion of P granules (outlined in red) under shear force (indicated by arrows, top left). These perinuclear granules, surrounding the nucleus (N, outlined in white), exhibit characteristic liquid-like behaviors over time, as shown at 0, 21, 32, 36, and 46 seconds. Reprinted with permission.[36] Copyright 2009, The American Association for the Advancement of Science.

This dynamic organization allows cells to rapidly adapt to environmental and metabolic changes.[47]

In gene regulation, LLPS drives the formation of transcriptional condensates at specific genomic loci. These condensates concentrate transcription factors, RNA polymerase, and other regulatory proteins, thereby enhancing the efficiency and specificity of gene expression.[19] The ability of these condensates to assemble and disassemble in response to signaling cues ensures that gene expression can be dynamically modulated to meet changing cellular demands.[48] LLPS also contribute to the formation of heterochromatin, where it organizes and silences large genomic regions. This LLPS-mediated chromatin organization restricts access to specific genes, enabling cells to regulate gene expression at a broader, genome-wide scale.[14] Biomolecular condensates are equally critical for cellular stress responses.[49] Stress granules, for instance, form under stress conditions such as heat shock or oxidative stress.[42]

These condensates temporarily sequester mRNA and translation-related proteins, preventing mRNA degradation and conserving cellular resources. Once the stress is alleviated, stress granules disassemble, releasing the sequestered mRNA for translation and enabling a rapid recovery of protein synthesis. This transient and reversible sequestration mechanism highlights the adaptive flexibility of condensates in protecting cellular functions under stress. Beyond gene regulation and stress responses, biomolecular condensates are also involved in the regulation of signaling pathways.[50] Signaling condensates form at the plasma membrane in response to receptor activation, where they concentrate signaling molecules to amplify and spatially constrain signaling events and ensure signaling precision.

The dynamic and responsive nature of biomolecular condensates makes them indispensable for maintaining cellular homeostasis. However, when the mechanisms governing LLPS

become dysregulated, condensates can transition from functional liquid-like states to pathological solid-like aggregates.[28] This aberrant phase behavior has been implicated in neurodegenerative diseases such as ALS, Alzheimer's disease, frontotemporal dementia (FTD), and Huntington's disease.[6,22] Understanding the molecular mechanisms that regulate LLPS is therefore critical not only for uncovering fundamental cellular principles but also for developing therapeutic approaches to mitigate diseases arising from condensate dysfunction.
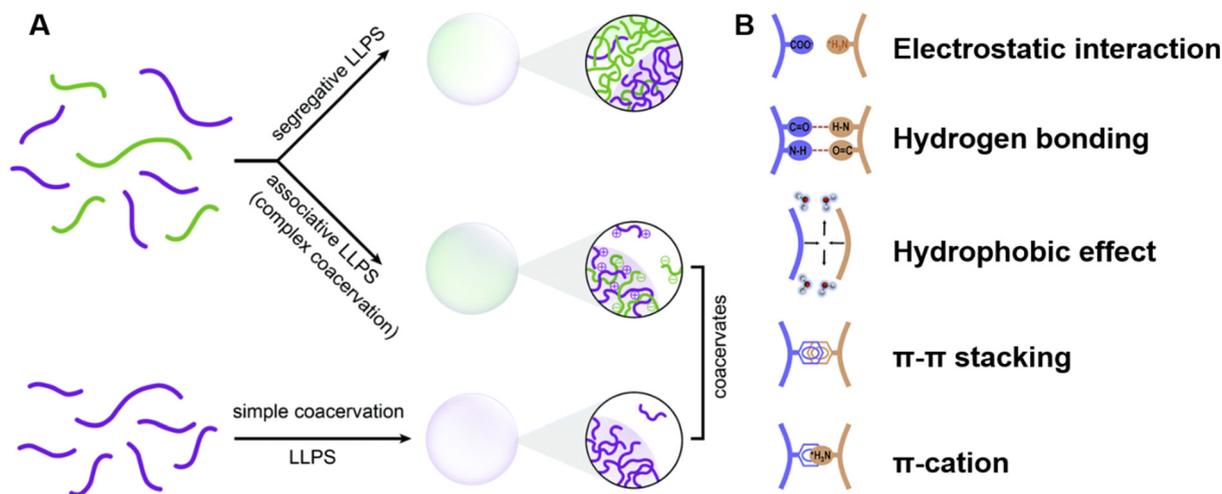
1.3. Peptide-mediated LLPS and coacervates

Peptide-mediated LLPS. Peptide-mediated LLPS is a rapidly growing research area that investigates how peptides self-assemble into dynamic liquid-like phases through weak molecular interactions.[51] Unlike proteins, peptides offer a simpler yet highly tunable platform for studying the fundamental principles of phase separation.[52] Depending on the components and the nature of molecular interactions, LLPS can be categorized into segregative LLPS, associative LLPS (complex coacervation), and simple coacervation (Fig. 3A), each with distinct mechanisms and applications.[53,54] Segregative LLPS occurs when mutual repulsion between soluble molecules drives their separation into distinct phases.[55] Associative LLPS, commonly termed complex coacervation, involves attractive interactions between different peptides that facilitate their complexation, resulting in a solute-rich phase and a solute-depleted phase.[56] In contrast, simple coacervation arises from the self-association of individual peptides, driven by intermolecular attractive interactions.[57] These processes are influenced by peptide sequence, length, and secondary structures,

such as α-helices or β-sheets, which can further determine whether peptide coacervates remain liquid-like states or transition into solid-like states.[53] Additionally, environmental factors like pH, temperature, and ionic strength modulate the stability and dynamics of peptide coacervates, making LLPS a versatile mechanism for both synthetic and biological applications.[56]

Examples and importance of peptide coacervates. Peptide coacervates are a key example of materials formed through LLPS, holding substantial importance in both scientific research and practical applications.[53,56] These coacervates result from the interactions of complementary charged peptides or intrinsic peptide properties, leading to the formation of dense, liquid-like phases capable of encapsulating bioactive molecules. A notable instance is seen with α-helical polypeptides, which, when combined with oppositely charged partners, form coacervates that remain stable despite environmental fluctuations, such as changes in salt concentration.[58] This stability is due to the structural characteristics of peptides, including charge density and conformational rigidity. Such stability is particularly advantageous in applications like drug delivery, where the ability to encapsulate and release therapeutic agents in a controlled manner is essential.[59–61] This level of control is especially valuable in treatments requiring localized delivery, like cancer therapy, where reducing side effects and maximizing therapeutic efficacy are critical goals.

Peptide-based coacervates can effectively encapsulate a variety of molecules, including nucleic acids, proteins, and small drugs, protecting them from degradation and facilitating their release in response to specific environmental stimuli.[62–65] The tunability of peptide sequences further enhances the utility

Fig. 3 Peptide-mediated liquid–liquid phase separation (LLPS) and coacervates. (A) Schematic representation of the types of LLPS that lead to the formation of coacervates. Segregative LLPS arises from repulsive interactions between distinct solute molecules, resulting in separate solute-enriched compartments. Associative LLPS, also known as complex coacervation, is driven by attractive interactions between solutes, forming coacervates enriched with multiple components. Simple coacervation involves the self-association of a single molecular species into dense, dynamic droplets. Reprinted with permission.[53] Copyright 2021 Royal Society of Chemistry. (B) Key molecular interactions driving peptide LLPS. The schematic highlights the primary interactions, including electrostatic interactions between charged residues, hydrogen bonding involving polar groups, hydrophobic interactions between nonpolar residues, π−π stacking between aromatic residues, and π-cation interactions between aromatic and positively charged residues. These interactions collectively determine the phase behavior and functional properties of peptide coacervates. Reprinted with permission.[51] Copyright 2023 Elsevier.

of these systems, allowing precise control over coacervate formation and dissolution to meet diverse functional requirements. Furthermore, the inherent biocompatibility and straightforward synthesis of peptides make them ideal candidates for developing new biomaterials and therapeutic platforms.[66,67] Their ability to form dynamic, responsive scaffolds that mimic the extracellular matrix supports cell growth and tissue regeneration, making them suitable for use in wound healing, cartilage repair, and other regenerative therapies. Additionally, the biodegradability of peptide-based materials ensures that they can be safely integrated into biological systems and eventually resorbed by the body.

In synthetic biology, peptide-mediated LLPS has been utilized to create artificial compartments and functional biomaterials.[65,68] These synthetic systems can be designed to perform specific tasks, such as catalyzing reactions or sequestering molecules, in a manner similar to natural cellular processes. The ability to engineer peptide-based coacervates with specific properties opens up new possibilities for the development of advanced materials that mimic or enhance natural biological functions. As research into peptide-mediated LLPS continues to advance, the potential applications of these systems in biotechnology and medicine are expected to grow, offering innovative solutions for drug delivery, tissue engineering, synthetic biology, and beyond. The ability to design and manipulate these systems at the molecular level holds great promise for enhancing our understanding of biological processes and developing novel therapeutic interventions.

1.4. Scope and objectives of the review

This review aims to provide a comprehensive overview of peptide-mediated LLPS, examining its implications in both biological systems and synthetic applications. The review seeks to elucidate the thermodynamic and molecular mechanisms driving peptide-mediated LLPS, explore how environmental factors such as pH, temperature, and ionic strength, influence phase separation, and analyze the transition of peptide coacervates from liquid-like to solid-like states. Furthermore, it will assess how external stimuli modulate LLPS and discuss the physicochemical properties of peptide coacervates, and their applications in drug delivery, tissue engineering, and synthetic biology. Through this detailed exploration, the review aims to enhance our understanding of peptide-mediated LLPS and underscore its potential for driving innovation in biotechnology and medicine.

2. Mechanisms of peptide-mediated LLPS

2.1. Thermodynamics and driving forces

The thermodynamics of peptide-mediated LLPS can be described using free energy considerations, where the system seeks to minimize its total free energy. The relevant free energy is the Gibbs free energy of mixing (ΔG_m), determined by both enthalpic (ΔH_m) and entropic (ΔS_m) contributions:

$$\Delta G_m = \Delta H_m - T\Delta S_m \qquad (1)$$

The enthalpy reflects the interaction potentials between peptide and solvent, while the entropy represents the available degrees of freedom for both peptide and solvent molecules. It is also crucial to recognize that the enthalpic contribution can be driven by specific molecular interactions, such as hydrogen bonding, aromatic stacking, or hydrophobic effects, depending on the peptide's sequence composition.[69] The mixing entropy specifically accounts for the entropic cost associated with confining peptide molecules in a dense phase. For phase separation to occur, the Gibbs free energy (ΔG_m) must be negative, indicating that the system can lower its energy by separating into two distinct phases, a peptide-rich dense phase, and a peptide-poor dilute phase. In LLPS, entropy generally favors a well-mixed state due to the greater number of possible configurations. However, the formation of a condensed phase results in a decrease in entropy, which must be compensated by a favorable enthalpic contribution, often driven by strong peptide–peptide interactions that replace less favorable peptide-solvent interactions. The thermodynamics of LLPS are influenced by the sequence-specific properties of the peptides, which can modulate the strength and nature of these interactions.[69] Additionally, the release of water molecules from the peptide surfaces into the bulk phase during condensate formation contributes an entropy gain that partially offsets the overall entropy loss, thereby facilitating phase separation.[70]

The Flory–Huggins theory extends the classical Gibbs free energy approach to describe the phase behavior of peptides in solution.[71,72] This theory considers the size difference between peptide and solvent molecules, as well as the specific interactions between them. In this model, the free energy of mixing is given by:

$$\frac{\Delta G_m}{k_B T} = \frac{\phi_p}{N}\ln\phi_p + \phi_s \ln\phi_s + \chi\phi_p\phi_s \qquad (2)$$

where ϕ_p and ϕ_s are the volume fractions of the peptide and the solvent, respectively. N corresponds to the length of the peptide. k_B is the Boltzmann constant and T is the temperature. χ is the Flory interaction parameter that quantifies peptide-solvent interactions. χ is further defined as:

$$\chi = \frac{z}{k_B T}\left[E_{ps} - \frac{1}{2}(E_{pp} + E_{ss})\right] \qquad (3)$$

where z is the coordination number, and E_{ps}, E_{pp}, and E_{ss} represent interaction energies per site for peptide-solvent, peptide-peptide, and solvent-solvent interactions, respectively.

The first two terms in eqn (2) account for the entropy change due to mixing, which is generally positive and favors mixing. However, for large polymers and peptides, this entropic contribution is relatively small due to the limited number of configurations available to these molecules. The third term represents the enthalpy of mixing, which may favor or oppose mixing depending on the sign and magnitude of χ. This parameter is highly sensitive to the specific sequence and chemical nature of the peptides involved, influencing their propensity for demixing under various conditions.

When charged peptides are involved, long-range electrostatic interactions significantly affect phase behavior. The Overbeek and Voorn extension of the Flory–Huggins model introduces a term related to charge density (σ) to account for these effects.[73]

$$\frac{\Delta G_{\mathrm{m}}}{k_{\mathrm{B}}T} = \frac{\phi_{\mathrm{p}}}{N}\ln\frac{\phi_{\mathrm{p}}}{2} + \phi_{\mathrm{s}}\ln\phi_{\mathrm{s}} - \alpha\left(\sigma\phi_{\mathrm{p}}\right)^{\frac{3}{2}} \qquad (4)$$

Here, σ represents the charge density, calculated according to Debye–Hückel theory, with α as a solvent constant determined by thermal energy $k_{\mathrm{B}}T$ and solvent molar volume. Strong interactions, typically lead to a first-order phase transition, resulting in two coexisting liquid phases. The extent of the two-phase region is modulated by interaction strength, which is further influenced by factors such as temperature, pH, peptide chemical groups, and salt concentration. In simple coacervation, the strength is primarily governed by χ, while in complex coacervation, it is determined by $\alpha\sigma^{3/2}$. Although the mean-field approach is a fundamental framework, it overlooks various factors like sequence specificity and nuanced interactions. Recent studies show that the sequence-dependent patterns of charged and aromatic residues can significantly alter the phase behavior, introducing complexities beyond the classical model.[69] While more advanced theories have been developed to address these complexities, they do not yet fully explain all types of LLPS in peptides, proteins, and polymers.[74] Consequently, the classical mean-field approach remains a valuable tool for understanding phase separation.

2.2. Molecular interactions in peptide-mediated LLPS

The multivalent forces driving peptide-mediated LLPS involve various molecular interactions, including electrostatic interactions between charged residues, hydrogen bonds involving polar groups, hydrophobic interactions between nonpolar residues, aromatic stacking (π–π) interactions between aromatic residues, and cation–π interactions between positively charged residues and aromatic groups (Fig. 3B).[5,51,75] These forces collectively contribute to the assembly and stabilization of peptide coacervates under different environmental conditions.

Electrostatic interactions. Electrostatic interactions are crucial for LLPS, especially in peptides with charged residues.[76] These interactions occur between oppositely charged amino acids, such as lysine, aspartate, or glutamate, forming ionic bonds that drive phase separation. In disordered RNA-binding proteins, for instance, electrostatic interactions between positively charged arginine residues and negatively charged RNA molecules promote the formation and stabilization of phase-separated droplets, which are essential for RNA processing and storage. The guanidinium group of arginine is particularly important because it facilitates strong electrostatic interactions. Substitution studies show that replacing arginine with lysine, which lacks the planar guanidinium group, significantly impairs LLPS.[35,77] Additionally, in mussel-derived peptides, the balance between attractive and repulsive electrostatic interactions is key to maintaining the liquid state of the coacervates under different

environmental conditions.[78] Adjusting pH or ionic strength significantly influences the LLPS behavior of these peptides, underscoring the importance of electrostatic forces in modulating phase behavior.

Hydrogen bonding. Hydrogen bonding is another key interaction that drives LLPS, especially in peptides containing amino acids capable of forming strong hydrogen bonds. In prion-like domains of RNA-binding proteins such as fused in sarcoma (FUS), tyrosine residues are indispensable for the formation and stabilization of condensates. Substitution studies reveal that replacing tyrosine with phenylalanine, which cannot participate in hydrogen bonding, impairs LLPS, while alanine substitution disrupts it entirely.[35] In histidine-rich peptides, hydrogen bonds between deprotonated histidine and tyrosine residues stabilize phase-separated droplets, acting as a molecular switch during LLPS.[78] In elastin-like polypeptides, hydrogen bonding between specific residues drives reversible phase separation, which underlies the formation of temperature-sensitive hydrogels. Similarly, in mussel-derived peptides, hydrogen bonds involving L-3,4-dihydroxyphenylalanine (Dopa) residues are critical not only for phase separation but also for determining the mechanical properties of coacervates.[79] The disruption of these bonds can lead to droplet dissolution, emphasizing their role in maintaining the structure and function of the peptide coacervates.

Hydrophobic effect. Hydrophobic effect is a major driving force in the LLPS of many peptides, driving the aggregation of hydrophobic amino acid residues to minimize their exposure to water, resulting in the formation of dense coacervate phases.[80,81] For example, in mussel-derived adhesive peptides, the hydrophobic effect is indispensable for the self-assembly of peptides into coacervates that enable robust underwater adhesion.[80] These interactions highlight the importance of hydrophobic residues in forming stable and functional peptide assemblies. Wu *et al.* further emphasize the influence of hydrophobic interactions on peptide phase behavior by using GY23, a synthetic peptide derived from mussel foot protein, as a model system.[82] Their study demonstrates that increasing hydrophobicity through targeted amino acid mutations (*e.g.*, alanine to phenylalanine) significantly enhances phase separation, reduces the critical concentration required for coacervation, and strengthens the viscoelastic properties of the resulting coacervates. These effects are further amplified by the formation of β-sheet structures, which stabilize the dense phase and enhance its mechanical robustness. Environmental factors, such as ionic strength and kosmotropicity, also modulate the strength of hydrophobic interactions. Higher ionic strength and kosmotropic salts promote phase separation by facilitating peptide-peptide interactions and enhancing hydrophobic effects.[82]

π–π interactions. π–π interactions, which occur between aromatic rings of amino acids such as phenylalanine, tyrosine, and tryptophan, play a fundamental role in peptide-mediated LLPS.[35,78] These interactions contribute to the structuring and stabilization of phase-separated droplets by facilitating tight aromatic stacking within the dense phase. For example,

in mussel-derived peptides, Dopa residues engage in π–π interactions that enhance cohesion within coacervates.[83] In synthetic peptides such as W_2R_2 and W_3R_3, π–π stacking among tryptophan residues drives the formation and compaction of coacervates, as evidenced by circular dichroism spectroscopy and molecular dynamics simulations.[84] Similarly, in low-complexity domains of RNA-binding proteins like FUS, tyrosine-mediated π–π interactions are critical for phase separation and condensate stabilization.[35] These interactions dictate the physical properties of the condensates and their functional versatility in both natural and engineered systems.

Cation–π interactions. Cation–π interactions occur between positively charged residues, such as arginine or lysine, and the electron-rich π systems of aromatic residues like tyrosine.[85–87] These interactions significantly influence the stability, dynamics, and structural organization of phase-separated droplets. Importantly, the specific chemical properties of these residues determine the strength and directionality of cation–π interactions, as highlighted in studies of FUS family proteins.[35,88] A study on FUS variants demonstrates the selective nature of cation–π interactions. Tyrosine-to-phenylalanine and arginine-to-lysine mutations revealed that phase separation is strongly driven by tyrosine–arginine interactions, with weaker contributions from tyrosine–lysine or phenylalanine–arginine pairs. This hierarchy emphasizes the importance of the planar guanidinium group of arginine, which enables delocalized electron–cloud interactions with aromatic residues, creating stronger and more directional cation–π interactions compared to the less delocalized amine group of lysine.[77] The driving forces for phase separation, quantified by saturation concentration, confirm the preference for tyrosine–arginine pairs over other combinations. These findings highlight that cation–π interactions are not merely generic electrostatic attractions but are dictated by the specific chemical structures of the interacting residues.

2.3. Role of amino acid sequence

While individual amino acids contribute to molecular interactions that drive and sustain LLPS, the sequence and arrangement of amino acids also determine the phase behavior and material properties of the resulting condensates.[57,89–92] Recent studies have revealed that proteins undergoing LLPS are intrinsically disordered or contain IDRs characterized by low-complexity sequences and enriched in polar, aromatic, proline, and glycine residues.[69,93–97] For example, peptides with repetitive arginine-glycine motifs exhibit a strong propensity for LLPS due to the molecular flexibility provided by glycine and the electrostatic interactions facilitated by arginine.[57] However, the number and distribution of these motifs are critical, as excessive repeats may increase electrostatic repulsion, hindering phase separation.[57,89,98] Histidine-rich beak proteins (HBPs) provide a notable example, with the presence of repetitive regions of low complexity amino acid sequence in their C-termini.[78] The motif repeat GHGLY drives the LLPS of HBPs and requires at least two copies and a linker sequence for broader phase separation conditions, such as variations in pH and salt concentration. Alternatively, four GHGLY tandem

repeats can independently trigger self-coacervation. LLPS can occur even in sequences lacking traditionally considered essential residues, such as charged or aromatic amino acids. For example, the peptide variant of $(GRGDSPYS)_{25}$ undergoes LLPS despite the absence of charged, aromatic, arginine, or glycine residues, challenging previous assumptions about strict sequence requirements.[89] The sequence not only dictates phase behavior but also impacts the material properties of condensates. $(GRGDSPYS)_{25}$ shows a viscosity of 11 Pa s, while the variants GRGASPYA and GRGNSPWS exhibit viscosities of 2 and 40 Pa s, respectively.

Contrary to earlier assumptions that LLPS requires a longer peptide sequence, LLPS can occur with ultrashort peptides, such as tetrapeptide W_2R_2 and hexapeptide W_3R_3, suggesting that phase separation is a general property of peptides, independent of sequence length.[84] These peptides undergo self-coacervation under specific conditions, such as high pH and sufficient concentration. Even shorter sequences, like dipeptide WR, can achieve LLPS through interactions with ATP. A comprehensive screening of 400 dipeptides derived from the 20 natural amino acids identified QW as a particularly promising LLPS candidate.[99] Both experimental and computational studies confirmed its strong phase separation potential. Other short peptides, such as *tert*-butyl diphenylalanine and methoxylated diphenylalanine derivatives, also exhibit LLPS capacity.[65,100] Additionally, the distribution of amino acid residues further influences LLPS behavior. For example, spacer sequences such as GSG, GLG, or SGS can promote, inhibit, or alter phase-separated structures.[101] Peptides with GLG spacers form liquid droplets, while those with GSG spacers remain soluble, and those with SGS spacers form aggregates and hydrogels. These findings emphasize the critical role of sequence and arrangement in determining phase behavior and material properties.

3. Methods for studying LLPS and biomolecular condensates

3.1. Experimental techniques

Fluorescence recovery after photobleaching. Fluorescence recovery after photobleaching (FRAP) is a straightforward method for assessing whether a biomolecular condensate exhibits liquid-like or solid-like properties.[39,102] It is also one of the few techniques available for measuring molecular diffusivity within biomolecular condensates *in vivo*.[103,104] FRAP involves using a high-power laser to selectively photobleach a specific region within a fluorescently labeled condensate and then monitoring the fluorescence recovery to evaluate the liquidity of condensates (Fig. 4A and B).[6,105] A short recovery time indicates a high exchange rate between the bleached region and its surroundings, suggesting high fluidity. In contrast, a prolonged recovery period reflects slower diffusivity, indicating reduced fluidity. This technique effectively distinguishes between different physical states, such as liquid-like droplets with rapid fluorescence recovery and solid-like or gel-like condensates where recovery is slower or incomplete.[104,106] FRAP has been extensively applied to study
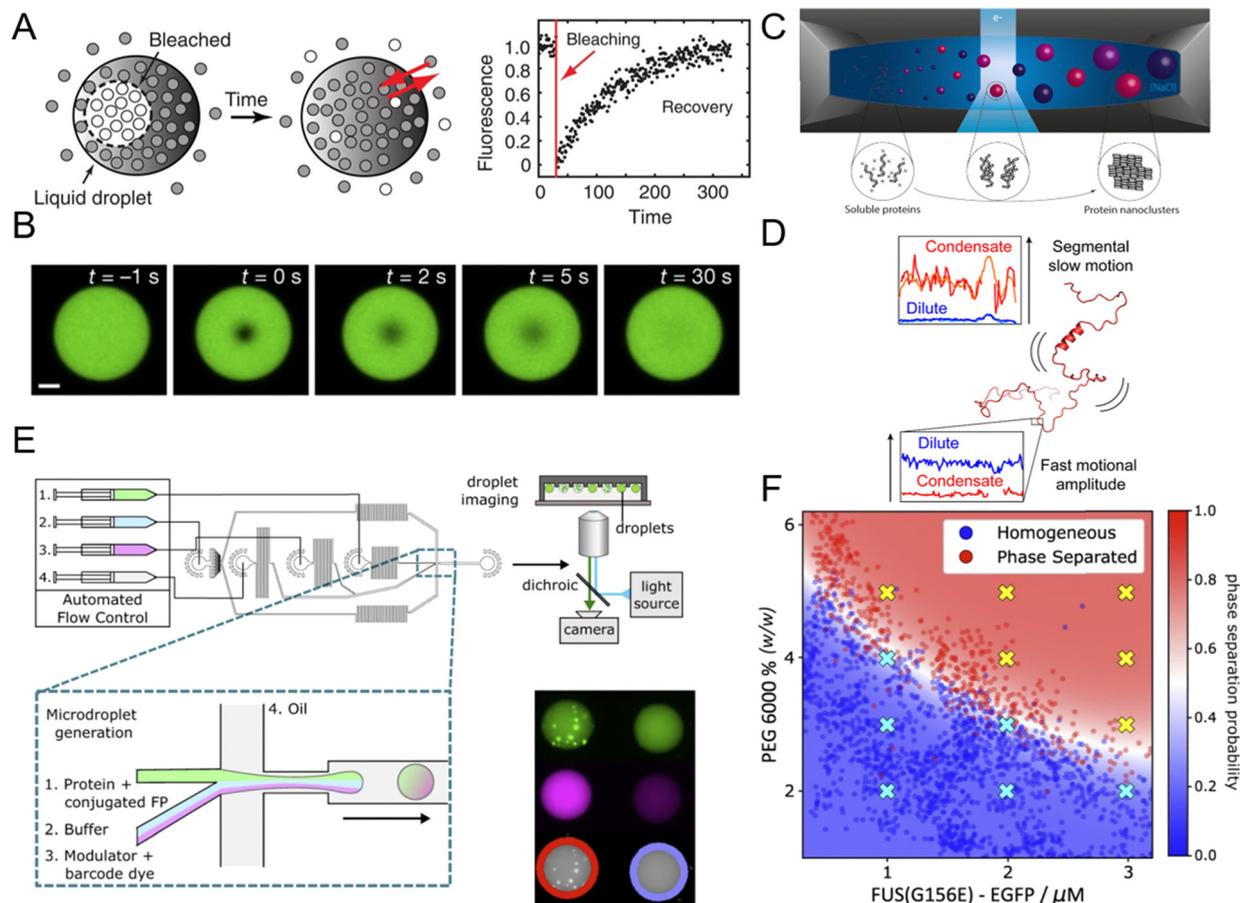
Fig. 4 Experimental techniques used to study liquid–liquid phase separation (LLPS) and biomolecular condensates. (A) Fluorescence recovery after photobleaching (FRAP) for evaluating the material properties and dynamics of biomolecular condensates. Following laser-induced photobleaching, fluorescence within the condensates gradually recovers, with a shorter recovery time indicating higher fluidity. Reprinted with permission.[6] Copyright 2017, The American Association for the Advancement of Science. (B) Fluorescence variation within a biomolecular condensate during a FRAP experiment. Scale bar, 5 µm. Reprinted with permission.[111] Copyright 2023 Springer Nature. (C) Schematic of a transmission electron microscopy (TEM) liquid cell used to study protein condensate formation and nucleation. Reprinted with permission.[112] Copyright 2019, American Chemical Society. (D) Example of nuclear magnetic resonance (NMR) spectroscopy demonstrating the differences in protein structure between the dilute and condensate phases. NMR spectroscopy can distinguish between atomic bond dynamics and overall molecular dynamics. Reprinted with permission under a Creative Commons Attribution 4.0 International License.[113] Copyright 2023 by the authors. (E) PhaseScan microfluidic setup for studying biomolecular condensates, where droplets with varying concentrations of proteins, buffer, and phase separation trigger solutions are generated *via* a flow-focusing technique, trapped in microwells, and analyzed using epifluorescence microscopy. (F) High-resolution phase diagrams generated by the PhaseScan microfluidic setup. (E) and (F) Reprinted with permission under a Creative Commons Attribution 4.0 International License.[114] Copyright 2022 by the authors.

the dynamics of various biomolecular condensates.[107–110] It has revealed that many condensates exist in a dynamic equilibrium, where molecules continuously exchange between the condensate and the surrounding solution (Fig. 4B).

Although FRAP is widely used, several limitations and challenges must be considered when interpreting FRAP data. A common misconception is the assumption that the recovery rate solely reflects the exchange rate between the dilute and dense phases. In reality, the recovery rate is also influenced by factors such as the size of the photobleached droplet, the mobility of molecules within the droplet, and the dimensions of the bleached area, which are often overlooked. Additionally, interpreting FRAP results requires careful consideration, especially for heterotypic condensates composed of multiple molecular species. In these cases, different components may exhibit

varying recovery behaviors due to distinct intermolecular interactions and spatial heterogeneities. The scaffold-client model explains this differential behavior, with scaffolds, which have multivalent binding capabilities, showing slower mobility compared to clients that interact through monovalent scaffold-binding modules.[37,115] Despite these limitations, FRAP remains popular due to its simplicity, accessibility, and convenience, offering a qualitative assessment of molecular diffusivity within condensates. FRAP is often used in conjunction with other techniques, such as fluorescence correlation spectroscopy and single particle tracking, to gain a more detailed understanding of the diffusion behavior and interaction networks within condensates.[103,115–117]

Microscopy. Microscopy techniques, particularly fluorescence and confocal microscopy, are foundational tools for visualizing

and analyzing LLPS in biological and synthetic systems.[118–120] Fluorescence microscopy allows for the specific labeling and tracking of molecules involved in phase separation, providing insights into their localization, concentration, and interaction within condensates. This technique is especially effective when using fluorescently tagged peptides or proteins, offering real-time observation of LLPS dynamics in living cells or *in vitro* systems. Confocal microscopy, which employs point illumination and a spatial pinhole to reduce out-of-focus light, is particularly useful for generating high-resolution images of LLPS in thick samples, enabling the reconstruction of three-dimensional structures. This capability is crucial for studying interactions between condensates and other cellular components, such as membranes and organelles.

Advanced imaging techniques, like super-resolution microscopy, extend the capabilities of conventional microscopy by surpassing the diffraction limit, allowing visualization of nanoscale structures within phase-separated droplets. Techniques such as stochastic optical reconstruction microscopy (STORM) provide detailed images of the internal organization of condensates, revealing substructures critical for understanding the molecular mechanisms driving LLPS.[121,122] In addition to offering information on physical dimensions like size, shape, and composition, advanced microscopy techniques also uncover material properties.[123] For instance, Brillouin microscopy, a noninvasive imaging modality, utilizes Brillouin light scattering principles to examine interactions between light and acoustic phonons, revealing intrinsic mechanical properties of biological samples at the microscopic scale.[124,125] This approach has been used to investigate the mechanical properties of protein aggregates formed through LLPS, which are relevant in neurodegenerative diseases.[126–128]

However, these techniques often rely on antibody staining or fluorescent labeling, which may alter the native state of biomolecular condensates. Electron microscopy (EM) offers an alternative by visualizing condensates with a high resolution (<10 nm) in a label-free manner. Cryo-electron microscopy (cryo-EM) captures snapshots of LLPS at cryogenic temperatures, preserving the native state of condensates and providing insights into their structural heterogeneity.[129,130] More recently, *in situ* liquid transmission electron microscopy (TEM) has been utilized to observe the dynamic process of LLPS in a time-resolved manner at the nanoscale (Fig. 4C).[112] This technique allows visualization of nucleation and growth of biomolecular nanoclusters, shedding light on the early stages of LLPS and the mechanisms behind the formation of biomacromolecular complexes. Collectively, these advanced microscopy techniques provide a comprehensive toolkit for studying the spatiotemporal dynamics of LLPS, from the initial nucleation of droplets to their maturation and interactions within the cellular environment.

Nuclear magnetic resonance and X-ray scattering. Nuclear magnetic resonance (NMR) and X-ray scattering techniques provide complementary insights into the molecular mechanisms underlying LLPS.[119,123,131–134] NMR spectroscopy is indispensable for probing atomic-level interactions and dynamics of peptides and proteins within both the dilute and condensed phases (Fig. 4D). This technique is particularly well-suited for studying IDRs, which are often the driving force behind LLPS due to their flexible conformations.[135] Pantoja *et al.* have used spatially resolved NMR to explore the internal structure of Tau protein condensates, revealing variations in concentrations of water, crowding agents, and protein cofactors within the condensates.[136] NMR can capture transient and weak interactions crucial for phase separation, including hydrophobic effects, hydrogen bonding, and aromatic stacking.[78] By analyzing chemical shifts, relaxation rates, and nuclear Overhauser effect signals, NMR provides a detailed picture of the conformational changes and interaction networks involved in LLPS.[78,137] Techniques like paramagnetic relaxation enhancement and residual dipolar couplings further enhance the ability of NMR to probe the structural ensembles of IDRs in phase-separated states, offering insights into how these proteins transition from a disordered to a more ordered state during condensate formation.

X-ray scattering techniques, particularly small angle X-ray scattering (SAXS), are invaluable for studying the overall shape, size distribution, and structural organization of peptide or protein complexes within phase-separated droplets.[78,138] SAXS provides nanoscale architectural information on parameters such as the radius of gyration, the degree of compactness, and the presence of higher-order assemblies, all critical for understanding the multivalent interactions and network formation within LLPS.[139,140] Beyond traditional SAXS, ultra-small angle X-ray scattering (USAXS) extends the range by capturing information about larger structures, bridging the gap between SAXS and conventional light scattering techniques.[141,142] USAXS is particularly useful for analyzing samples with features spanning several orders of magnitude in size, offering structural insights over a wide range of length scales. Furthermore, combining SAXS with NMR and cryo-EM allows for a comprehensive understanding of both the static and dynamic aspects of LLPS, integrating structural and functional studies of biomolecular condensates.[143] However, challenges remain, such as the need for high sample concentrations to achieve adequate signal strength and the risk of biomacromolecule damage from energetic beam sources. These techniques also struggle to probe highly disordered regions and may not fully capture the size and complexity of some condensates.

Microfluidics and high-throughput techniques. Microfluidics platforms have revolutionized the study of LLPS by providing precise control over experimental conditions and enabling systematic exploration of phase behavior under various environmental settings.[102,114,123,144–147] These devices manipulate small volumes of fluids, typically from femtoliter to microliter scale, within microfabricated channels, allowing to create and to study phase-separated droplets in a controlled environment (Fig. 4E). The advantages of microfluidics include reduced cost, precise spatial and temporal control of analyte concentrations, higher experimental throughput, compact device size, and the capability to integrate with other techniques like optical tweezers and microscopy for enhanced biochemical control.

A significant advancement in this field is the integration of high-throughput screening capabilities with microfluidic

platforms. For example, droplet-based microfluidics generates thousands of microdroplets, each containing different concentrations of peptides. Automated imaging and analysis tools monitor these droplets, enabling comprehensive exploration of phase diagrams across a wide range of conditions using specialized microfluidic chip designs.[114,148–151] Arter *et al.* developed the PhaseScan platform, a combinatorial droplet microfluidic system for rapid, high-resolution acquisition of multidimensional biomolecular phase diagrams (Fig. 4F).[114] This platform automates droplet generation, trapping, and imaging, significantly reducing experimental time and minimizing potential errors by eliminating manual preparation and imaging of individual conditions. This high-throughput technique facilitates the mapping of LLPS conditions, accelerating the discovery of new phase-separating systems and optimizing the conditions for specific phase behaviors.

Emerging technologies within microfluidics continue to push the boundaries of LLPS research. Innovations such as serpentine microchannels allow for continuous observation of droplets over extended periods, while controlled shear stress application provides insights into the dynamic behavior of phase-separated systems.[114,147,152] In addition, microfluidic platforms enable experimental methods not feasible with traditional bulk assays, such as measuring the zeta potential of individual droplets, a critical parameter for understanding surface charge properties.[153] These advancements improve our understanding of the physical properties of condensates, and allow for simulating complex biological environments where LLPS is pivotal.[154,155] By combining microfluidics with other high-resolution imaging techniques, it is possible to explore LLPS dynamics under near-physiological conditions and provide a more accurate representation of *in vivo* systems.

3.2. Computational approaches

Computational approaches have become indispensable in the study of peptide-mediated LLPS, providing insights at scales that are challenging to achieve experimentally. This part focuses on two main computational methodologies: molecular dynamics simulations, and bioinformatics and machine learning tools.[99,156,157] Both approaches offer unique advantages in understanding the complex interactions that drive LLPS.

Molecular dynamics simulations offer a detailed atomistic view of peptide interactions and their roles in LLPS.[89,99] By simulating the behavior of peptides under varying conditions, molecular dynamics simulations allow for the exploration of the thermodynamics and kinetics of phase separation. Yang *et al.* have employed molecular dynamics simulations to investigate the phase separation of repetitive polyproline and polyarginine peptides with varying lengths and sequences.[158] This study highlighted the critical role of sequence order and peptide length in promoting LLPS. It demonstrated that peptides with fewer than ten polyarginine repeats did not exhibit LLPS, even at high salt concentrations. The simulations revealed that both hydrophobic and electrostatic interactions are crucial drivers of phase separation, aligning well with experimental observations. Molecular dynamics simulations can also explore the effects of external

factors, such as temperature and salt concentration, on LLPS.[158] For example, the same study showed that increasing salt concentration enhances LLPS by reducing electrostatic repulsion between charged residues. Similarly, temperature variations were shown to modulate the conformational entropy of peptides, thereby affecting their ability to undergo phase separation. As the number of known phase-separating proteins and peptides grows, bioinformatics and machine learning tools have become increasingly important for predicting LLPS behavior based on sequence data.[157,159,160] These tools leverage large datasets to identify patterns and features that correlate with LLPS propensity, enabling the prediction of novel phase-separating systems. One notable example is the PSPredictor tool, developed by Chu and coworkers.[157] PSPredictor uses a machine learning algorithm trained on sequence data from the LLPSDB database to predict phase-separating proteins (PSPs). The tool combines componential and sequential information during protein embedding, achieving a high accuracy of 94.71% in cross-validation tests. By providing predictions that are not dependent on specific protein types, PSPredictor facilitates the identification of novel scaffold proteins for biomolecular condensates and other phase-separated structures. Machine learning approaches like PSPredictor are particularly powerful because they can process vast amounts of sequence data, uncovering hidden relationships between sequence features and phase behavior. These tools are invaluable for guiding experimental studies, identifying candidates for further investigation, and expanding our understanding of the sequence determinants of LLPS.

4. Physicochemical properties and environmental effects on peptide coacervates

4.1. Materials properties of peptide coacervates

Viscosity and elasticity. Viscosity and elasticity are critical parameters defining the mechanical properties of peptide coacervates, influencing their behavior and functionality in both biological and synthetic systems.[82,161,162] Viscosity refers to the resistance of a coacervate to flow under an applied force, indicating its fluidity. Elasticity, on the other hand, describes the ability of a coacervate to return to its original shape after deformation, reflecting its ''springiness'' or capacity to resist permanent structural changes. The viscosity of peptide coacervates is influenced by various factors, including peptide concentration, molecular weight, and the nature of interactions among peptides.[89] Higher peptide concentrations generally increase viscosity because the dense network of interactions restricts molecular mobility. This effect is particularly pronounced in coacervates formed from peptides rich in charged residues or those capable of forming multiple hydrogen bonds, as these interactions create an interconnected, entangled network that resists flow and enhances viscosity. As illustrated in Fig. 5A, the viscosity of biomolecular condensates (0.1–100 Pa s), including those formed by proteins such as LAF-1, FUS, and NPM1, suggest a polymer-based aqueous two-phase system
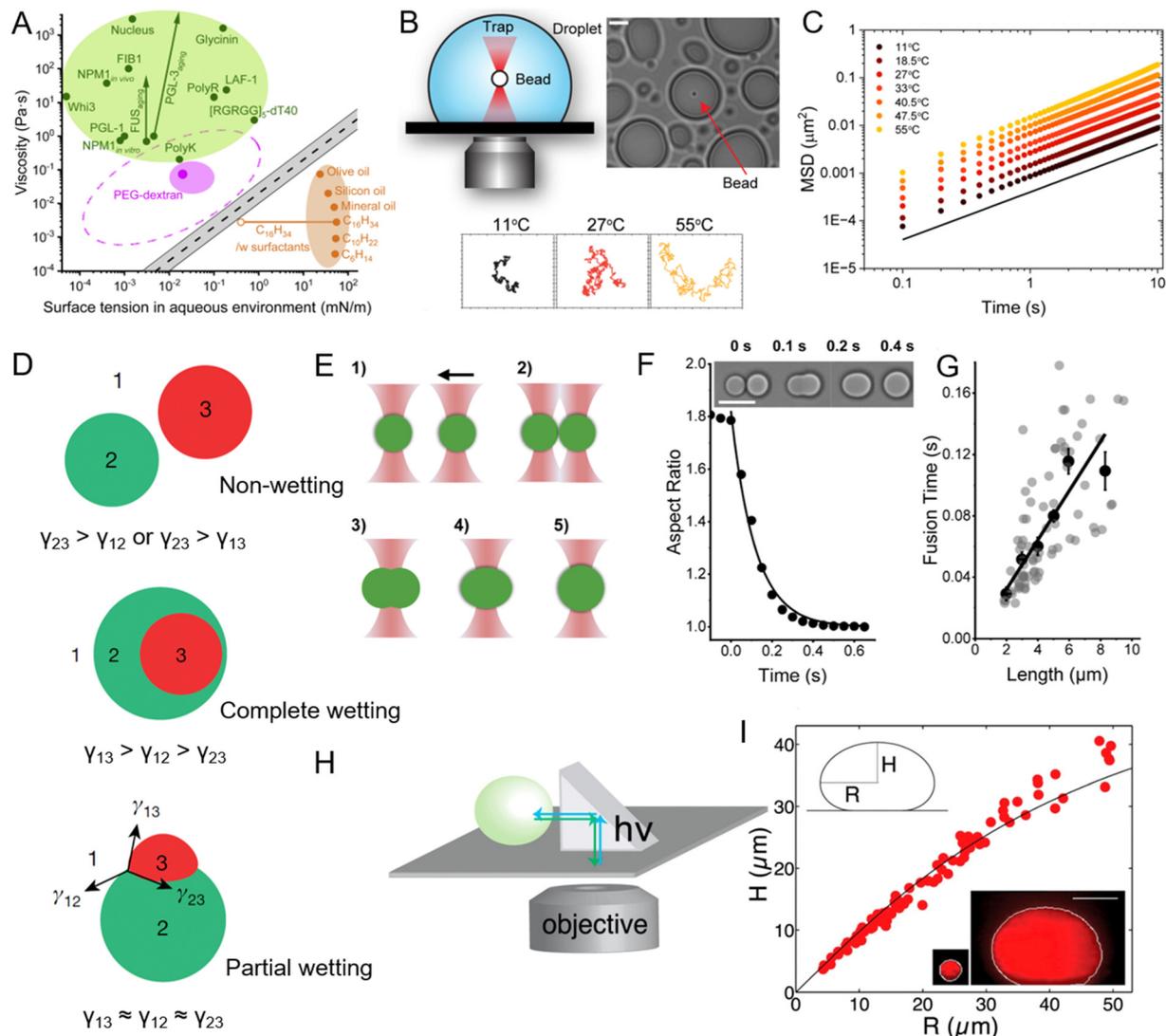
Fig. 5 Viscosity and surface tension of peptide coacervates and the experimental methods used to measure these physicochemical properties. (A) Comparison of viscosity and surface tension of biomolecular condensates in aqueous buffer, PEG-dextran coacervate systems, and common ''oil droplet'' in water. Reprinted with permission under a Creative Commons Attribution 4.0 International License.[163] Copyright 2021 by the authors. (B) Schematic of the experimental setup for passive microrheology with optical tweezers to measure the viscosity of peptide coacervates, with representative particle trajectories recorded at three different temperatures. (C) Ensemble-averaged mean squared displacements (MSD) of 200-nm beads within peptide coacervate at varying temperatures. (B) and (C) Reprinted with permission under a Creative Commons Attribution 4.0 International License.[169] Copyright 2024 by the authors. (D) Different modes of multiphase droplet structuring based on relative interfacial tensions. In case of high interfacial tension between two droplets (γ_{23}), droplets remain separate (upper). When the 1-3 interface is energetically costly, phase 2 envelopes phase 3 (middle). When the relative energetic costs are balanced, all three phases may share interfaces (lower). Reprinted with permission.[167] Copyright 2022, Springer Nature. (E) Illustration of the coacervate fusion experiment using dual-optical traps. (F) Fusion of two peptide coacervates (inset images) shown as a decrease in aspect ratio to 1. Scale bar, 10 μm. (G) Fusion time of peptide coacervates as a function of coacervate size, where the slope of the linear fit corresponds to the inverse capillary velocity, η/γ, with η representing viscosity and γ surface tension. (E)–(G) Reprinted with permission under a Creative Commons Attribution 4.0 International License.[163] Copyright 2021 by the authors. (H) and (I) Schematic of XZ imaging of biomolecular condensates using a right-angle prism (H) and the relationship between height and radius of nucleoli at steady state (I), used to determine the surface tension of the condensates. The shape of a biomolecular condensate resting on a surface is determined by a balance between surface tension, which favors the formation of round droplets, and gravitational forces, which tend to flatten droplets. Surface tension can be determined by analyzing the droplet's profile in the XZ dimension. The black line indicates the fit from the average surface tension for all condensates. Reprinted with permission.[109] Copyright 2016, Elsevier.

rather than simple oil–water interfaces.[163–166] This resemblance to polymer physics provides a framework for understanding the behavior of peptide coacervates, where the dense network of interactions results in slow capillary velocity and

high resistance to deformation. Elasticity is closely related to the molecular architecture of the peptides and proteins. Condensates containing proteins with IDRs often display significant elasticity due to the flexibility and dynamic nature of

these regions, allowing them to stretch and recover without permanent deformation. Functionally, the balance between viscosity and elasticity is crucial in determining how peptide coacervates respond to mechanical stress and interact with their environment. In biological systems, this balance is essential for processes like intracellular transport, where condensates must be fluid enough to move through the cytoplasm while maintaining structural integrity when encountering obstacles.[167] In synthetic applications, controlling viscosity and elasticity is vital for drug delivery systems, where coacervates must encapsulate and release therapeutic agents in response to environmental stimuli.[168]

Several methods have been employed to study the viscosity and elasticity of peptide coacervates. Among these, rheology serves as a primary technique for measuring the flow and deformation behavior of coacervates under various stress or strain conditions.[170] Microrheology, which usually combines with optical tweezers, tracks the motion of embedded tracer particles and offers a localized understanding of viscoelastic properties on a microscopic scale (Fig. 5B and C).[169,171,172] In addition, micropipette aspiration technique, has enabled direct measurement of viscosity in biomolecular condensates.[163,173,174] Advances in microfluidic technology further enable precise manipulation and measurement of coacervate properties under controlled conditions. These platforms allow for the generation of droplets with defined sizes and compositions, where viscosity and elasticity can be systematically varied and measured in real time, providing valuable insights into the mechanical properties of coacervates in environments that closely mimic cellular conditions.[154]

Surface tension. While the role of biomolecular condensates as cellular compartments has been widely studied, their ability to create interfaces with surrounding cytoplasm, adjacent condensates, and cellular structures is less explored. These interfaces generate interfacial or capillary forces.[167,175] In non-living soft matter systems, such interfaces are crucial for organization, shaping the topology of multiphase liquids, and determining the structure and geometry of soft materials.[176,177] Surface tension is a fundamental property that governs the stability, shape, and interfacial behavior of peptide coacervates (Fig. 5D).[84,167] It arises from the imbalance of molecular forces at the interface between the coacervates and its surrounding environment, leading to tendencies such as minimizing surface area, coalescence, or maintaining shape across various environments. Surface tension in peptide coacervates is highly sensitive to the composition and structure of the peptides, as well as environmental conditions such as ionic strength, pH, and temperature.[178] Fig. 5A shows the relationship between surface tension and viscosity across various systems, including biomolecular condensates, PEG-dextran coacervates, and common oil–water interfaces. Biomolecular condensates, such as those formed by proteins like LAF-1 and FUS, exhibit surface tension values ranging from 10^{-4} to 10^{-1} mN m^{-1}, which are significantly lower than those observed for oil–water interfaces. This distinct characteristic aligns biomolecular condensates more closely with PEG-dextran coacervates, whose surface tensions are within a similar range. Surface tension also stabilizes coacervates by influencing droplet fusion, fission, and wetting behavior, processes essential for their function in both biological and synthetic systems.[109,179] In cellular environments, the ability to adjust surface tension allows coacervates to adapt to osmotic pressure changes, interact with membranes, or merge with other condensates, facilitating processes such as cargo sequestration, signal transduction, and compartmentalization.[162,168]

To study surface tension, several experimental techniques are commonly used. Micropipette aspiration is a key method where a droplet of the coacervate is aspirated into a micropipette, and the pressure required to deform the droplets is measured, allowing for the calculation of surface tension.[163] Dual optical traps provide a precise method for measuring the surface tension of biomolecular condensates by studying their fusion dynamics (Fig. 5E–G).[163,180,181] In this approach, two condensates are individually controlled using optical traps and brought into contact (Fig. 5E). Upon releasing one condensate, the fusion process occurs under the influence of viscosity and surface tension. High-speed imaging captures the process, and changes in the aspect ratio of the condensates are analyzed to extract the fusion time using a single exponential decay model (Fig. 5F). The geometric mean of the condensate diameters defines their length, allowing the ratio of viscosity to surface tension (inverse capillary velocity) to be estimated from the fusion time *versus* length relationship (Fig. 5G). The right-angle prism imaging technique is another powerful method for determining the surface tension of biomolecular condensates (Fig. 5H).[109] By imaging the *XZ* plane of condensates, this technique measures their radius and height, enabling the application of the Young-Laplace equation to calculate surface tension.[182] As shown in Fig. 5I, when a coalesced droplet flattens at the bottom of the nucleus under gravity, the extent of flattening is countered by surface tension, providing key data for its measurement. Using this approach, the surface tension of the outermost granular component of the nucleolus was determined to be approximately 0.4 µN m^{-1}. Similarly, the method was employed to measure the surface tension of purified nucleophosmin droplets *in vitro*, yielding a value of around 0.8 µN m^{-1}.[109] These remarkably low surface tension values indicate the liquid-like, immiscible behavior of nucleolar subcompartments. Atomic force microscopy (AFM) can also be used to measure the forces required to deform a droplet directly, offering insights into both surface tension and mechanical properties.[178] Together, these methods provide a comprehensive understanding of surface properties, guiding the design of coacervate systems with tailored properties for specific applications.
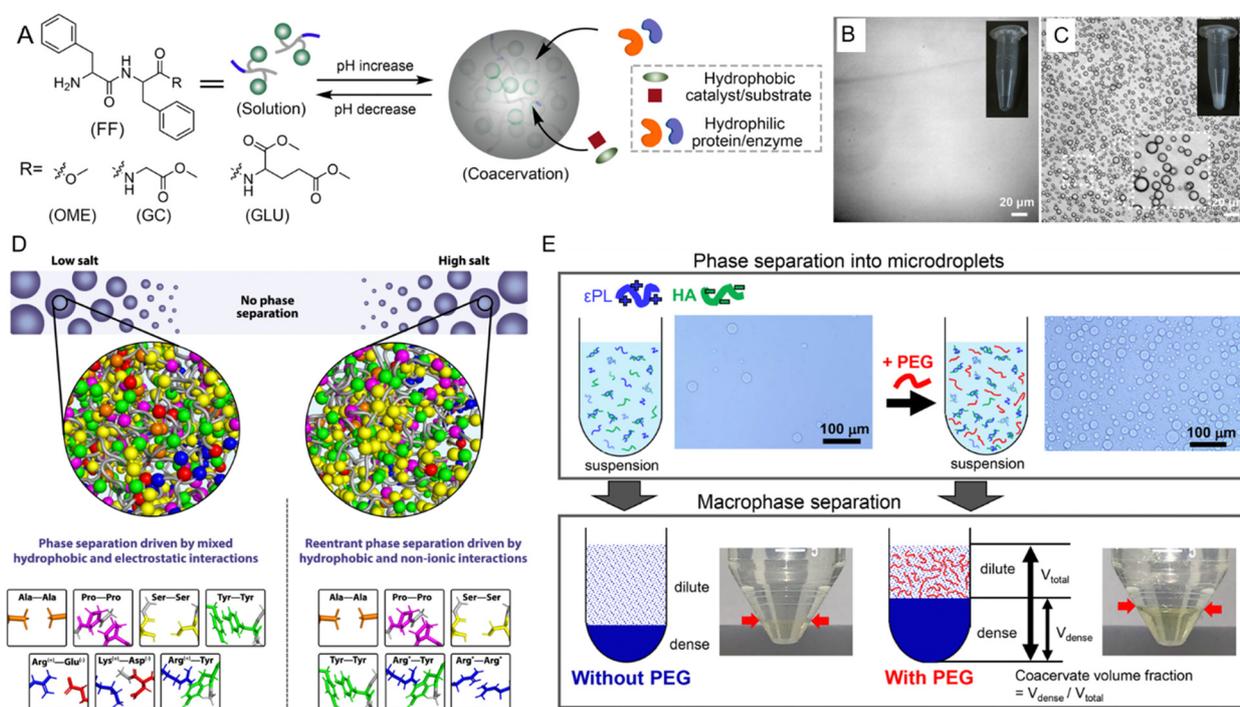
4.2. Environmental effects on LLPS

The formation and stability of peptide coacervates are highly sensitive to environmental conditions such as pH, temperature, ionic strength, and molecular crowding.[183–186] Understanding how these factors influence LLPS is crucial for deciphering the mechanisms that regulate coacervate behavior both *in vivo* and *in vitro*.

pH. pH can modulate the ionization state of amino acids and thereby affect electrostatic interactions that drive LLPS.[184,187] Changes in pH can significantly alter the net charge of peptides, which in turn modulates their intermolecular interactions. For example, lowering the pH can lead to the protonation of acidic residues such as glutamate and aspartate, reducing the overall negative charge and decreasing electrostatic repulsion. This change promotes molecular clustering and facilitates phase separation. Conversely, increasing pH can result in deprotonation of basic residues, such as lysine and arginine, enhancing electrostatic repulsion and potentially disrupting existing condensates. In synthetic systems, pH-sensitive peptides can be designed to assemble or disassemble in response to environmental pH changes, offering controlled strategies for drug delivery and therapeutic release. The effects of pH on LLPS are also demonstrated by the self-coacervation behavior of dipeptide components, such as diphenylalanine capped with a methoxy group (FF-OMe), which undergo LLPS in response to pH changes (Fig. 6A). When the pH is lowered to 6, the FF-OMe solution remains clear and homogeneous, indicating the dipeptides are fully soluble in the aqueous buffer (Fig. 6B). However, when the pH is increased to 9, the FF-OMe dipeptides undergo phase separation, forming spherical coacervate droplets (Fig. 6C). This reversible pH-triggered LLPS behavior is distinct from the irreversible fiber formation observed with other amphiphilic FF derivatives. The phase transition is also concentration-dependent, with higher concentrations of FF-OMe allowing droplet formation at lower pH values. This behavior is attributed to the structural features of FF-OMe, which has a less hydrophilic head group and a more flexible tail compared to other FF derivatives, thus promoting LLPS under specific pH conditions.

Temperature. Temperature is another vital factor that modulates LLPS by influencing the thermodynamics of intermolecular interactions.[183] The temperature-dependent behavior of phase-separating systems is typically categorized into two principal models: upper-critical-solution-temperature (UCST) and lower-critical-solution-temperature (LCST) phase behaviors.[10,190–192] UCST phase separation occurs below a specific threshold temperature, where reduced thermal energy enhances interactions such as cation–π, π–π stacking, and electrostatic forces.[193] These interactions dominate over entropy, promoting molecular clustering and phase separation. In contrast, LCST phase behavior is driven by hydrophobic effects, where increasing the temperature above a critical threshold reduces the entropic

Fig. 6 Environmental effects on liquid–liquid phase separation (LLPS) of peptides. (A) Schematic representation of pH-triggered LLPS involving dipeptide components. (B) Micrographs showing diphenylalanine capped with a methoxy group (FF-OMe) in solution at pH 6. (C) Micrographs showing an FF-OMe coacervate dispersion at pH 9. (A)–(C) Reprinted with permission under a Creative Commons Attribution 4.0 International License.[65] Copyright 2024 by the authors. (D) Schematic of molecular forces stabilizing condensates in low-salt *versus* high-salt regimes. In low-salt conditions, phase separation is driven by both electrostatic and hydrophobic interactions, while in high-salt regimes, hydrophobic and nonionic interactions dominate. Asterisks (*) for Arg*-Tyr and Arg*-Arg* indicate that at high salt concentrations, charges are screened, and interactions become predominantly hydrophobic. Reprinted with permission under a Creative Commons Attribution 4.0 International License.[188] Copyright 2021 by the authors. (E) Schematic of LLPS in a system of ε-polylysine (ε-PL) and hyaluronic acid (HA) with and without PEG. Microdroplet coacervate suspension was observed *via* optical microscopy, with macrophase separation occurring after centrifugation. Reprinted with permission under a Creative Commons Attribution 4.0 International License.[189] Copyright 2020 by the authors.

penalty of water solvating protein backbones.[194] This promotes the release of solvent molecules, enabling phase separation through entropy gain. For UCST-driven LLPS, intrinsically disordered proteins such as resilin-like polypeptides demonstrate the importance of aromatic residues and positively charged residues.[195] These residues enhance intermolecular interactions, driving phase separation under colder conditions. In LCST systems, exemplified by elastin-like polypeptides, phase separation is primarily governed by hydrophobicity.[196,197] Increasing the hydrophobicity of guest residues lowers the could-point temperature, promoting phase separation at elevated temperatures.[198] Biological systems utilize UCST and LCST behaviors to adapt to environmental changes. UCST-driven phase separation supports protective compartmentalization during cold stress by enhancing molecular clustering. Conversely, LCST behavior facilitates responses to heat shock, mitigating protein aggregation and denaturation.[10] The combination of UCST and LCST elements in chimeric sequences enables dual thermoresponsive behavior.[10,183,199] These chimeric systems exhibit distinct phase transitions across temperature regimes, integrating the strengths of both mechanisms. Such dual-responsive designs have significant potential in synthetic applications. For example, thermally responsive biomolecular condensates could serve as smart materials for drug delivery, releasing therapeutic agents in response to specific temperature changes. Additionally, biomaterials engineering could leverage these principles to develop adaptive systems with precise thermal control over phase separation.

Ionic strength. Ionic strength significantly influences LLPS by modulating electrostatic interactions between charged molecules.[79,80,82] In systems dominated by electrostatic interaction, such as those involving nucleic acids or highly charged peptides, ionic strength significantly affects the stability, dynamics, and material properties of condensates. At low ionic strength, strong electrostatic attractions between oppositely charged molecules facilitate the formation of phase-separated droplets. However, as ionic strength increases, surrounding ions screen these interactions, reducing the propensity for phase separation. This screening effect is particularly relevant in cellular environments, where fluctuating ion concentrations dynamically regulate the assembly and disassembly of biomolecular condensates. The influence of ionic strength varies depending on the type of ions present and their position in the Hofmeister series.[82] Kosmotropic ions, such as sulfate (SO_4^{2-}), stabilize phase separation by enhancing hydrophobic and π–π interactions, while chaotropic ions, such as bromide (Br^-), disrupt phase separation by weakening these interactions. These ion-specific effects illustrate how different ions can modulate the molecular forces driving LLPS. Beyond specific ion types, the general impact of ionic strength is exemplified by NaCl, where increasing concentrations from 0.1 to 2 M in GY23 peptide coacervates reduced electrostatic repulsion and strengthened π–π stacking between tyrosine residues. This resulted in an increase in storage modulus by nearly an order of magnitude and enhanced adhesive force. Similarly, for the GK-16 peptide derived from mussel adhesive proteins, higher

ionic strengths promoted a transition from liquid to gel-like states, driven by reduced electrostatic repulsion and increased peptide chain associations.[79] These results underscore the dual role of ionic strength, influenced both by the nature of specific ions and their concentrations, in programming the viscoelastic properties of peptide coacervates. Fig. 6D schematically illustrates the role of ionic strength in regulating molecular interactions within biomolecular condensates.[188] In the low-salt regime, phase separation is driven by electrostatic and hydrophobic interactions. In contrast, at high salt concentrations, reentrant phase separation occurs, governed primarily by hydrophobic and nonionic interactions such as π–π stacking, involving both aromatic and non-aromatic residues. This reentrant phase behavior highlights the plasticity of molecular driving forces for LLPS, which are influenced not only by amino acid composition but also by environmental conditions.

Molecular crowding. Molecular crowding, a defining feature of the cellular interior, is a significant factor influencing LLPS.[185,200,201] The crowded environment within cells, where macromolecules such as proteins, nucleic acids, and polysaccharides are densely packed, can drastically alter the thermodynamics and kinetics of phase separation. Crowding agents such as PEG mimic this intracellular environment by promoting LLPS through volume exclusion and depletion effects.[185,189,200] These agents effectively increase the local concentration of phase-separating molecules, enabling phase separation even at lower concentrations. Fig. 6E shows PEG enhances the stability and density of coacervates formed by ε-polylysine (ε-PL) and hyaluronic acid (HA).[189] Without PEG, these coacervates form unstable microdroplets, but the addition of 10% (w/v) PEG significantly increases their yield and density by concentrating polyelectrolytes within the dense phase. Molecular crowding also influences the dynamic properties of condensates. Increased PEG concentration can transition ribonucleoprotein condensates from liquid-like to gel-like states by strengthening the intermolecular network.[202] FRAP studies show reduced protein mobility within condensates as PEG concentration rises, indicating enhanced depletion interactions and structural rigidity. Similarly, crowding-induced dehydration of polyelectrolytes increases entropy, favoring coacervation and stabilizing condensates, even under high salt conditions. Furthermore, molecular crowding reshapes the thermodynamic landscape of LLPS. For example, in bovine γD-crystallin systems, PEG raises the phase separation temperature, reflecting stronger attractive interactions between proteins.[203] Such flexibility in LLPS mechanisms highlights the ability to tune condensate properties through the selection of specific crowding agents and conditions.

4.3. Phase behavior and transition mechanisms

Phase diagrams. Phase diagrams are essential tools for visualizing the conditions under which a mixture of components separates into distinct phases.[197,198] Fig. 7 shows the fundamental principles of LLPS by depicting a phase diagram that delineates the boundaries between one-phase and two-phase regimes.[2] The diagram highlights critical thresholds such as the binodal line, where phase separation begins, and the spinodal region,
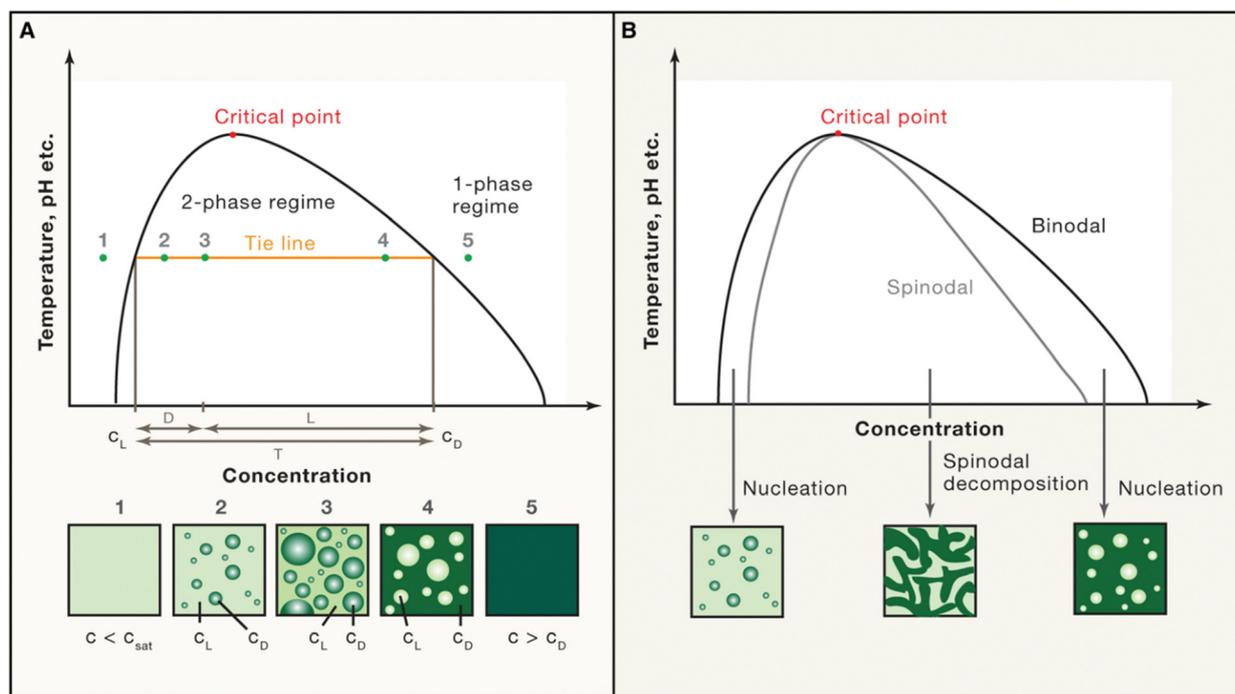
Fig. 7 Schematic phase diagram. (A) and (B) The phase diagram shows the coexistence line (black), which delineates the boundary between the one-phase and two-phase regimes, influenced by environmental factors such as temperature and pH. Beyond the critical point, phase separation does not occur. (A) Below the saturation concentration (c_{sat}), the system remains in the one-phase regime. In the two-phase regime, the system separates into a light phase (c_L) and a dense phase (c_D), with fixed concentrations along a tie line (orange). Volume fractions of each phase can be calculated using the lever rule. (B) The spinodal curve (grey) marks the region of instability where spinodal decomposition occurs. Between the coexistence line (binodal) and the spinodal, phase separation requires nucleation. Reprinted with permission.[2] Copyright 2019 Elsevier.

characterized by spontaneous demixing due to its instability. The critical point, marking the transition beyond which LLPS does not occur, is also shown. Tie lines connect points representing the compositions of coexisting dilute and dense phases in the two-phase region, indicating equilibrium conditions and phase proportions determined by the lever rule. These graphical elements collectively provide a comprehensive understanding of the thermodynamics driving LLPS.

The most common phase diagrams used in LLPS studies are temperature-concentration diagrams, where the *x*-axis represents the concentration of the biomolecules, and the y-axis represents the temperature. These diagrams often feature binodal curves that define the coexistence region, where the system separates into a dense phase and a dilute phase. The binodal curve comprises two arms: the left arm represents the saturation concentration in the dilute phase, while the right arm indicates the concentration in the dense phase (Fig. 7). Constructing accurate phase diagrams for LLPS requires precise experimental techniques to measure biomolecule concentrations in both phases across various temperatures and conditions. Traditional methods include optical microscopy, turbidimetry, and light scattering to determine the cloud-point temperature (the temperature at which phase separation begins at a fixed concentration) or the saturation concentration (the concentration at which phase separation occurs at a fixed temperature).[2,204–206] Recent advances have introduced high-throughput techniques like droplet microfluidics, which allow label-free extraction of complete phase diagrams in finite volumes.[102,114,145] This method confines solutions in micro-sized compartments, enabling precise measurement of dense phase volume and binodal lines. In addition to experimental approaches, theoretical models, such as the Flory–Huggins theory, are also employed to fit experimental data and predict phase behavior.[9] These models account for the free energy of mixing and interaction parameters between different components, providing a framework for understanding the thermodynamics of LLPS. Combining experimental data with theoretical models enables to construct comprehensive phase diagrams that accurately capture the conditions for phase separation.

Phase diagrams have far-reaching applications in biological research and material science.[3,207,208] In biology, they are used to understand the formation and regulation of membraneless organelles. Mapping the phase behavior of peptides and proteins under various conditions provides insights into the mechanisms driving the assembly and disassembly of these condensates.[3,207] In material science, phase diagrams guide the design of smart materials, such as temperature-responsive polymers and drug delivery systems, which leverage LLPS for encapsulating and releasing therapeutic agents in response to environmental triggers.[209,210]

Overall, phase diagrams are indispensable for understanding the conditions under which LLPS occurs, providing a window into the thermodynamic and kinetic properties of phase-separating systems. The construction and interpretation

of these diagrams, through both experimental and theoretical approaches, are crucial for advancing our knowledge of biomolecular condensates in cells and for designing materials with novel functionalities. As research continues to refine these tools, phase diagrams will continue to be central to LLPS studies, offering critical insights into the behavior of complex systems in both natural and synthetic contexts.

Transition from liquid-like to solid-like states. As mentioned above, biomolecular condensates, also known as membrane-less organelles, are dynamic assemblies of biomolecules formed through LLPS.[5] A defining characteristic of these condensates is aging, which refers to their gradual transition from a liquid-like state to a more solid-like or arrested state over time.[106,211–213] Aging plays a pivotal role in cellular functions, such as stress adaption and molecular regulation, while also contributing to pathological conditions, including neurodegenerative diseases and cancer.[5,28,214] Initially, condensates exhibit viscoelastic properties that enable rapid assembly, disassembly, and exchange of molecular components.[36,41,215] However, as they age, their material properties evolve, with increased viscosity and relaxation time signaling a gradual shift toward solid-like states, resembling behaviors observed in glass-forming systems.[216]

The aging of biomolecular condensates is governed by structural and biochemical factors. Proteins with IDRs promote LLPS through transient molecular interactions that maintain fluidity.[217] Post-translational modifications, such as phosphorylation and methylation, further stabilize these interactions, delaying the transition to solid-like states.[88,218–220] In their absence, condensates age more rapidly, leading to aggregation and functional decline.[2,187] Structural changes, including the formation of β-sheet-rich regions or multiphase architectures like gel-core/liquid-shell configurations, contribute to aging by introducing localized molecular order.[221] These transitions, driven by enhanced interprotein interactions, progressively stabilize the solid-like state and alter the dynamics of condensates. Proper regulation of aging is critical for preserving the functionality of biomolecular condensates. Besides the post-translational modification, the loss of the liquid-like character of condensates during aging can be modulated by biochemical processes and amino acid sequence mutations.[106,212,213] Understanding the regulatory mechanisms is crucial for developing therapeutic strategies to mitigate pathological aging. By targeting molecular interactions, biochemical pathways, or energy-dependent processes, it may be possible to prevent or reverse aberrant transitions, preserving the dynamic and functional nature of biomolecular condensates.

Peptide self-assembly through LLPS provides a unique opportunity to explore the transition from liquid-like to solid-like states in synthetic systems.[51,56,222–225] Unlike the classical theory describing a direct liquid-to-solid transition, Fig. 8A illustrates the nucleation and growth process of supramolecular nanofibrils mediated by LLPS.[130] Initially, a homogeneous solution of amphiphilic amino acids or short peptides undergoes phase separation into solute-rich and solute-poor liquid phases. The solute-rich liquid droplets serve as precursors for nanofibril nucleation, with hydrated nanoclusters acting as nucleation loci. This phase separation is primarily entropy-driven, with the favorable entropy contribution likely originating from the expulsion of water from the liquid droplets. These solute-rich liquid droplets create specialized microenvironments that, lower the nucleation barrier compared to classical nucleation pathways and facilitate the assembly of highly ordered nanostructures. The transition from metastable liquid droplets to thermodynamically stable nanofibrils is mediated by enthalpic interactions and follows Ostwald's step rule.[226] Fig. 8B shows the dynamic evolution of Ag^+-coordinated 9-fluorenyl-methoxycarbonyl (Fmoc)-Ala nanofibrils from liquid droplets to solidified intermediates and ultimately to mature nanofibrils.[130] Cryo-TEM images show the formation of dense liquid droplets that coalesce over time, while solidified droplets exhibit increased contrast, signifying structural reorganization. Fibril-like protrusions emerge from the droplet, marking the transition to more stable, thermodynamically favorable nanofibrils. The inset SEM image further corroborates the elongation of fibrils from the droplet surface, demonstrating the progression from metastable liquid intermediates to ordered fibrillar structures.

The self-assembly of peptides into nanostructures through LLPS is influenced by multiple factors. Recent studies using synthetic coacervates and *in vitro* reconstitution systems have provided valuable insights into the mechanisms underlying the liquid-to-solid transition in LLPS.[53,106] For example, chemically fueled reaction cycles have been utilized to control the liquidity of droplets, allowing precise tuning of the material state of condensates.[227] These systems highlight the importance of both thermodynamic and kinetic factors to fully understand and predict the behavior of LLPS under different conditions. Additionally, advanced imaging techniques, such as FRAP and super-resolution microscopy, provide real-time insights into the dynamics of condensates as they transition between liquid-like and solid-like phases.[228] These techniques reveal that even within a single condensate, different regions may display varying degrees of liquidity or solidity, reflecting the complex and heterogeneous nature of these structures.

The study of peptide self-assembly through LLPS not only advances our understanding of fundamental processes driving phase separation but also offers insights into the design of biomimetic materials with tunable properties. By controlling environmental conditions such as temperature, pH, and ionic strength, the material state of condensates can be fine-tuned, making them useful for applications in biomaterial engineering, drug delivery, and disease treatment. The transition from liquid-like to solid-like states in LLPS is governed by a complex interplay of molecular interactions, environmental conditions, and cellular regulation. Understanding how these transitions occur is essential for elucidating the dynamics of biomolecular condensate and developing therapeutic interventions for diseases linked to aberrant phase transitions.

4.4. Influence of external stimuli on LLPS

LLPS is a highly dynamic process that cells can finely tune in response to various external stimuli, allowing rapid adaption to
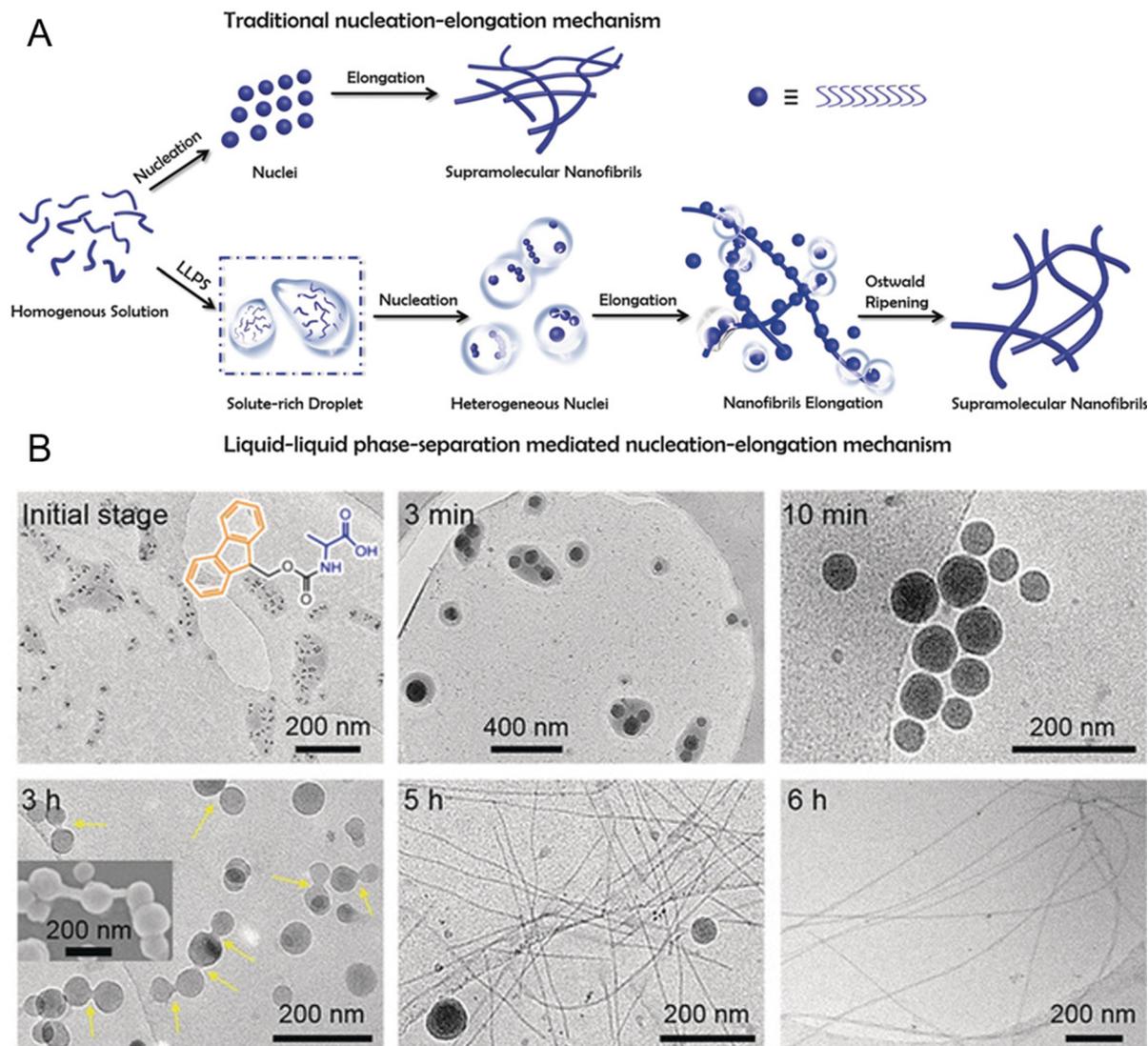
Fig. 8 Formation of supramolecular nanofibrils *via* liquid–liquid phase separation (LLPS)-mediated nucleation and self-assembly of peptides. (A) Schematic of the self-assembly process of supramolecular nanofibrils from amino acids or short peptides, where LLPS precedes nucleation, with solute-rich droplets serving as nucleation precursors for fibril formation following Ostwald's step rule, which is different from the traditional nucleation-elongation mechanism. (B) Cryo-TEM images of the dynamic evolution process of Ag^{+}-coordinated 9-fluorenylmethoxycarbonyl (Fmoc)-Ala self-assembling nanofibrils over time. These images demonstrate the structural evolution from the amino acid-dense liquid droplets to the metastable solidified droplets and, finally, to thermodynamically favorable nanofibrils through LLPS, nucleation, and subsequent nucleation-elongation processes. Reprinted with permission.[130] Copyright 2019 Wiley-VCH Verlag KGaA.

changing environmental conditions. Among the most impactful stimuli are light, redox changes, and mechanical forces, each capable of modulating the assembly, disassembly, and material properties of phase-separated condensates.[152,229–231] By influencing these properties, external stimuli play a pivotal role in the structural and functional regulation of biomolecular condensates.

Light. The ability of light to control LLPS and the assembly and disassembly of biomolecular condensates has opened new avenues for manipulating cellular processes.[230,232,233] Light-responsive LLPS systems typically utilize optogenetic clustering techniques to induce reversible transitions between liquid-like and solid-like states in condensates, providing spatial and temporal control over phase behavior.[234,235] The optogenetic clustering systems, including optoDroplets, optoClusters, and PixELLs, harness light to regulate the oligomerization state of peptides or proteins, enabling the dynamic formation and dissolution of liquid-like droplets or more rigid clusters.[230,234] Fig. 9A illustrates the optoDroplets and optoClusters systems, which are based on the Cry2 protein. The optoDroplets, formed by Cry2 fused to the IDR of FUS, are liquid-like droplets that rapidly exchange monomers, while optoClusters, created by the Cry2 variant, form more stable, rigid clusters that do not exchange subunits with the solution.[230,234] This optogenetic approach enables precise control over the assembly of LLPS droplets, with the potential to tune the material properties of
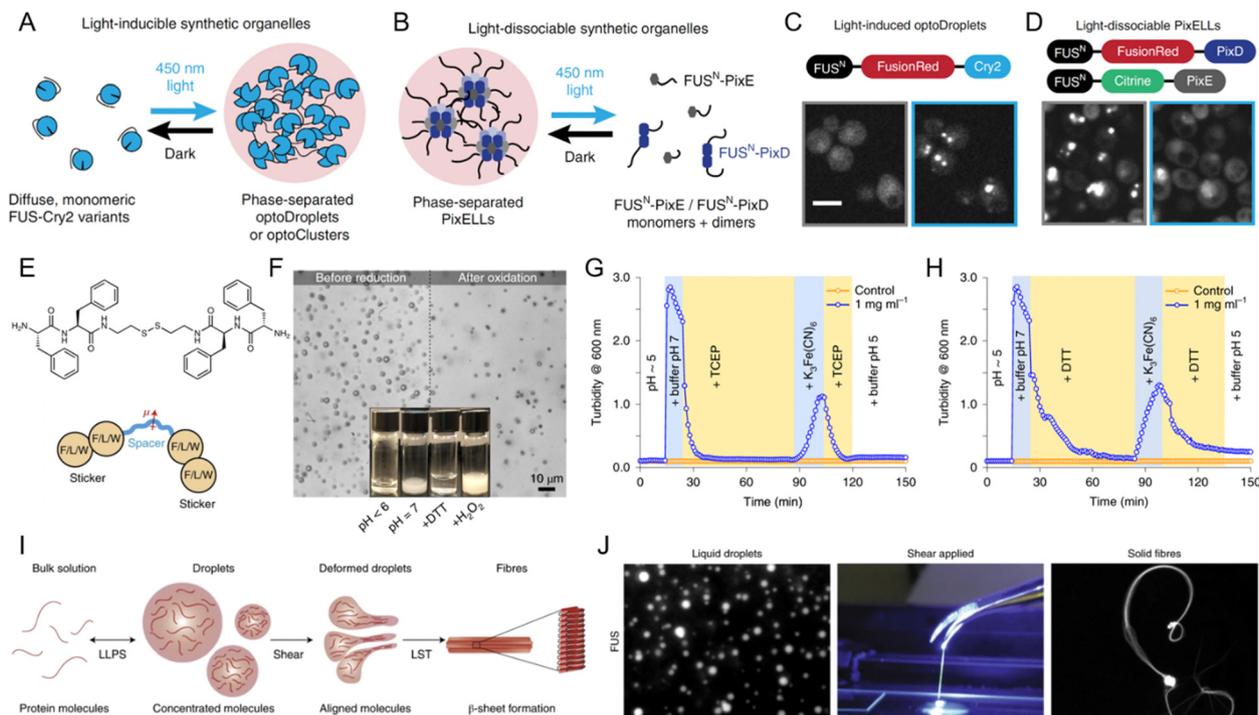
Fig. 9 Influence of external stimuli on liquid–liquid phase separation (LLPS). (A)–(D) Light-mediated control of biomolecular condensate formation. (A) and (C) FUS proteins fused to variants of the Cry2 optogenetic system trigger phase separation in the optoDroplet and optoCluster systems upon exposure to 450 nm light. (B) and (D) FUS fusion to the PixD/E proteins enables the formation of the PixELL optogenetic system, which dissociates under 450 nm light. Scale bar, 5 μm. (A)–(D) Reprinted with permission.[230] Copyright 2019 Springer Nature. (E)–(H) Redox regulation of LLPS. (E) Structure of bis(phenylalanyl–phenylalanyl) cystamine (FFssFF) and schematic illustration of the synthon motif with two dipeptide stickers and a polar spacer. (F) Formation and dissolution of FFssFF coacervate droplets before reduction and after oxidation. (G) Kinetics of coacervate dissolution upon reduction with tris(2-carboxyethyl) phosphine (TCEP) and reformation through condensation upon oxidation with $K_3Fe(CN)_6$, as measured by turbidity. (H) Similar kinetics observed with dithiothreitol (DTT) as a reducing agent. (E)–(H) Reprinted with permission.[238] Copyright 2021 Springer Nature. (I) and (J) Influence of shear force on LLPS-driven biomolecular condensates. (I) Schematic and experimental data showing the formation of β-sheet-rich fibers from condensate droplets under shear force. (J) Formation of FUS solid fibers under shear forces. Reprinted with permission.[152] Copyright 2020 Springer Nature.

the condensates. Fig. 9B demonstrates the PixELLs system, based on the PixD and PixE from *Synechocystis*, where co-expression of FUSN-PixD and FUSN-PixE results in the formation of liquid-like droplets that can be rapidly disassembled upon blue light exposure.[230] This system shows the potential of light to modulate LLPS dynamically, enabling real-time control over condensate behavior. These systems have proven useful in regulating engineered metabolic pathways in yeast, where the assembly and disassembly of synthetic organelles, such as enzyme-containing condensates, can be controlled by light. This allows for rapid, post-translational control of biochemical reactions, improving the efficiency of microbial production processes in bioreactors. Fig. 9C and D further illustrate the reversible nature of light-induced LLPS transitions. In these experiments, optoDroplets and PixELLs exhibit light-dependent changes in oligomerization, with optoDroplets transitioning between diffuse and clustered states upon light stimulation (Fig. 9C), while PixELLs undergo light-induced dissociation, moving from stable clustering in the dark to a more dispersed state upon light exposure (Fig. 9D). The dynamic switching between these phases is not only valuable for studying cellular dynamics but also for controlling protein localization and

activity within cells, offering new tools for targeted drug release and therapeutic applications.[232] The use of light-responsive LLPS systems holds great promise in a wide range of applications, from optogenetics to drug delivery. Light-activated phase-separating molecules, such as those with azobenzene or other photochromic groups, change shape upon exposure to specific wavelengths of light, enabling the precise tuning of condensate formation.[236,237] This non-invasive control of LLPS provides new possibilities for spatiotemporal protein clustering, targeted therapeutic delivery, and the study of intracellular processes in real time. These systems are expected to offer significant advances in synthetic biology, biochemistry, and medicine, with the ability to fine-tune condensate formation and dissociation for various biological and therapeutic applications.

Redox change. Redox changes play a pivotal role in regulating LLPS both in cellular environments and synthetic systems, influencing the formation and dissolution of biomolecular condensates.[238–240] In cells, the redox state directly impacts phase separation, particularly under oxidative stress or during crucial processes such as autophagy and apoptosis.[241] During oxidative stress, for instance, phase-separated condensates can

solidify to sequester damaged proteins, thereby protecting cellular components from further degradation. This dynamic behavior highlights the importance of LLPS in cellular stress responses, where the ability of condensates to transition between liquid-like and solid-like states ensures the proper management of misfolded or damaged proteins. Moreover, redox-sensitive LLPS systems, including those with cysteine residues or other redox-active motifs, hold significant therapeutic potential.[231] In disease contexts, shifts in the cellular redox state can trigger the selective release of drugs from redox-responsive biomolecular condensates, offering a targeted approach to treatment.[62,239] In this way, redox-modulated LLPS serves as both a biological sensor and a therapeutic tool, playing a central role in cellular health and disease management.

In synthetic systems, redox changes are similarly crucial for modulating LLPS and controlling the formation of peptide coacervates. Redox-sensitive groups, such as disulfide bonds, undergo reduction or oxidation, causing structural changes in proteins or peptides that influence their phase separation behavior. Fig. 9E illustrates the structure of bis(phenylalanyl–phenylalanyl) cystamine (FFssFF) peptide derivative, which consists of two phenylalanine dipeptide "stickers" and a polar cystamine "spacer".[238] This peptide derivative undergoes redox-induced phase separation, with the reduction and oxidation of disulfide bonds playing a critical role in driving coacervation. Fig. 9F shows the reversible behavior of FFssFF coacervates, with droplets dissolving after reduction and reforming after oxidation. Fig. 9G demonstrates the reduction of the disulfide bond using tris (2-carboxyethyl) phosphine (TCEP), resulting in the dissolution of coacervates into a clear solution. Upon oxidation with potassium ferricyanide ($K_3Fe(CN)_6$), the coacervates reform, demonstrating the reversibility of this redox-induced coacervation. This process is not limited to TCEP, as shown in Fig. 9H, where dithiothreitol (DTT) is used as the reducing agent and the same reversible coacervation behavior is observed. These findings underscore the versatility of redox-responsive systems, where the ability to control phase separation in synthetic systems mirrors the dynamic behavior seen in biological condensates. By leveraging redox chemistry, researchers can design systems with precisely tunable LLPS behavior, expanding the potential applications of biomolecular condensates in both fundamental research and therapeutic strategies.

Mechanical forces. Mechanical forces, such as shear stress or compression, are also known to have a profound impact on the behavior of biomolecular condensates, influencing their properties and structural transitions.[211,242] These forces can shift condensates from a fluid-like to a more solid-like state by reorganizing the molecular networks. This adaptability to mechanical cues is particularly important for cells experiencing continuous mechanical forces, such as muscle cells, cartilage, and vascular endothelial cells. LLPS under mechanical stress may alter condensate viscoelasticity, impacting cellular processes like mechanotransduction, where cells convert mechanical signals into biochemical responses.[243] Fig. 9I illustrates the effects of shear on the formation of fibers from protein condensates. In this proposed model, protein molecules first concentrate into liquid droplets through LLPS.[152] When shear forces are applied, the polypeptide chains within the droplet align, facilitating intermolecular interactions. These interactions lead to the formation of β-sheet-rich fibers, transforming the liquid condensates into solid structures. This fiber formation process is similar to that observed in silk spinning, where proteins undergo a shear-mediated transition to solid fibers.[244] Supporting this concept, Fig. 9J shows the behavior of FUS protein condensates under mechanical shear. LLPS of FUS was induced by reducing the salt concentration, after which shear forces were applied using tweezers.[152] This manipulation resulted in the extraction of solid fibers from the FUS droplets. Notably, microfluidic experiments have revealed that a critical shear stress of approximately 0.5 Pa is necessary to trigger this transition, a value within the range of shear stresses found in biological systems, such as cytoplasmic streaming and axonal transport.[245,246] The influence of mechanical stress on LLPS is of particular importance in tissue subjected to frequent or intense mechanical forces. LLPS under mechanical stress can contribute to cellular resilience by stabilizing condensates, which in turn protect critical molecules from physical deformation. Moreover, varying mechanical conditions can influence the kinetics of phase transitions, affecting the size, shape, and internal organization of condensates. These findings have significant implications in synthetic biology, particularly for developing LLPS-based materials that mimic the adaptive responses of biological systems. Such materials hold potential for tissue engineering and regenerative medicine, where mimicking the dynamic nature of cellular responses to mechanical forces is a valuable goal.

5. Applications of peptide-mediated LLPS and biomolecular condensates

5.1. Biomaterials and tissue engineering

Peptide-mediated LLPS and biomolecular condensates have gained significant attention in recent years as promising tools in the field of biomaterials and tissue engineering. These systems offer unique properties such as environmental responsiveness, tunable mechanical strength, and the ability to encapsulate bioactive molecules, which make them highly suitable for various applications, including bioadhesives, tissue repair, biocomposites, and dynamic scaffolds.[155,247–252] Inspired by natural processes, peptide coacervates have the potential to create highly adaptable materials that can be customized to meet the specific needs of different biological applications.

One of the most promising applications of peptide or protein-based biomolecular condensates is their use as bioadhesives for soft and hard tissue repair.[253,254] Traditional adhesives often fall short of meeting the mechanical and biological requirements for effective tissue integration. However, peptide coacervates offer a solution by mimicking the adhesive properties of natural systems. Fig. 10A shows the bioinspired condensates composed of recombinant mussel adhesive protein (rMAP) and hyaluronic acid (HA).[247] These rMAP-HA
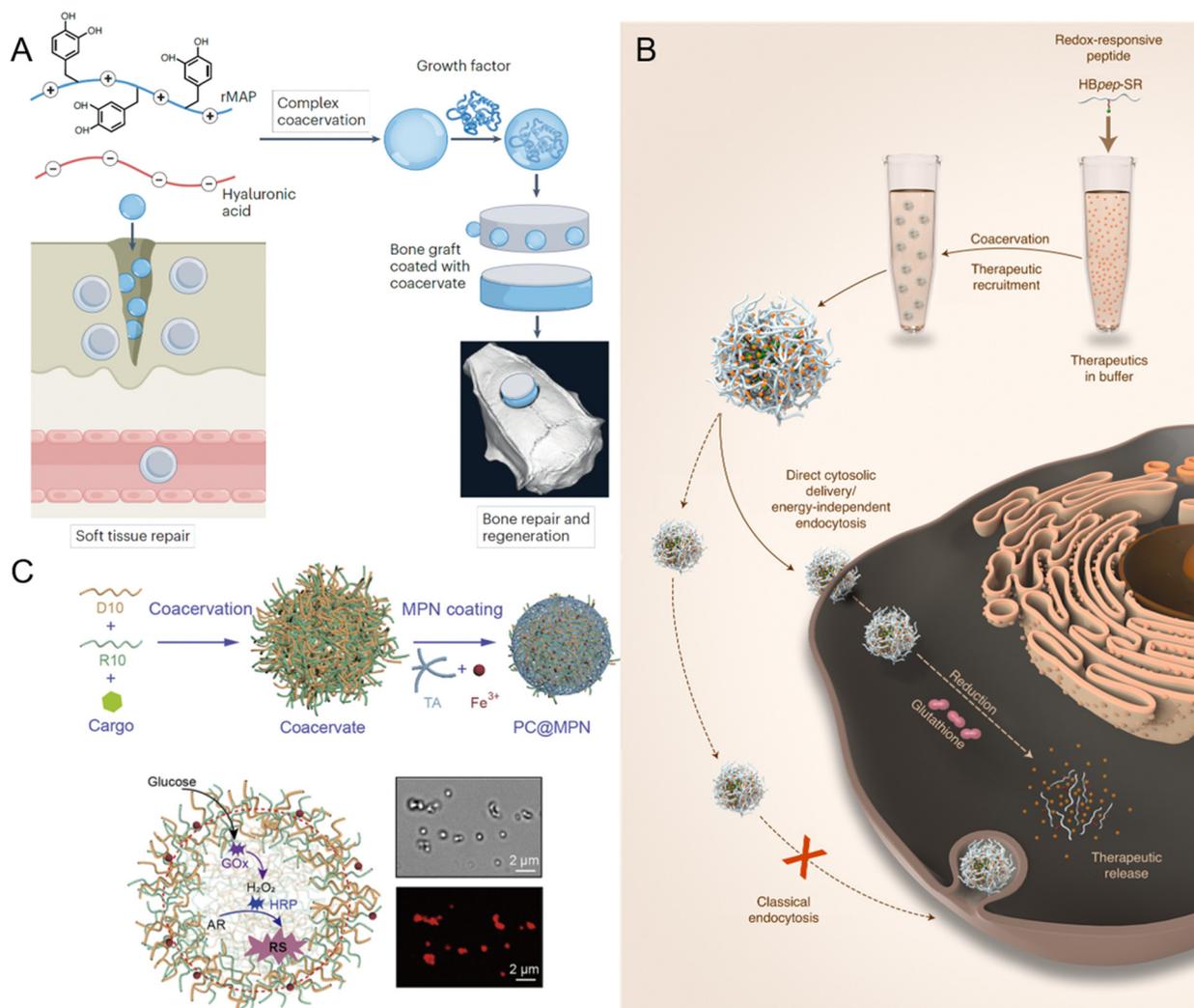
Fig. 10 Applications of peptide-mediated liquid–liquid phase separation (LLPS) and biomolecular condensates in various fields. (A) Application of recombinant mussel adhesive protein (rMAP) and hyaluronic acid (HA) coacervates for tissue engineering, including soft tissue repair and bone regeneration *via* growth factor recruitment. Reprinted with permission.[247] Copyright 2024 Springer Nature. (B) Design of redox-responsive peptide coacervates for direct cytosolic drug delivery. Histidine-rich beak peptides conjugated with a lysine residue and a self-immolative moiety (HBpep-SR) undergo coacervation, encapsulating macromolecular therapeutics. Upon incubation with cells, the therapeutics-loaded coacervates enter the cytosol, where intracellular glutathione triggers coacervate disassembly and drug release. Reprinted with permission.[258] Copyright 2022 Springer Nature. (C) Fabrication of membrane-bound protocells (PC@MPN) with emergent properties, achieved by coating peptide coacervates (PCs) with metal-phenolic networks (MPNs). The protocell facilitates enzymatic cascade reactions, where glucose oxidase (GOx) converts glucose to H_2O_2 and horseradish peroxidase (HRP) catalyzes the oxidation of Amplex Red (AR) to resorufin (RS), as indicated by red fluorescence. Reprinted with permission.[259] Copyright 2023 American Chemical Society.

condensates not only outperform their individual components in terms of adhesive performance but also promote cell proliferation when applied to implant surfaces. This cell growth is essential for tissue integration, a key factor in the success of medical devices or implants. Further modifications, such as the fusion of rMAP with low-complexity mammalian sequences, improve the adhesive strength by forming stronger, amyloid-like nanofibrils that firmly adhere to surfaces.[255] In addition to enhancing adhesive strength, these coacervates also support tissue repair. Their viscous, water-immiscible nature makes them suitable for sealing tissues and promoting healing. For example, rMAP-HA condensates have been successfully used to

seal urinary fistulas, which is a difficult clinical issue, and have shown potential as skin grafts for wound healing.[253,256] Moreover, these condensates have been applied as binders for bone xenografts, aiding in bone regeneration.[254,257] Their ability to encapsulate and release growth factors, such as bone morphogenetic protein 2, further enhances their regenerative potential by simulating tissue regeneration and promoting healing at the site of injury.[254] This versatility makes bioinspired coacervates a powerful tool for advanced tissue repair technologies.

Peptide coacervates also offer significant potential as dynamic scaffolds in tissue engineering.[260] The mechanical properties, such as stiffness and flexibility, can be tuned by modifying

the peptide sequence, allowing for the creation of scaffolds tailored to specific tissue types. HBPs derived from squid have shown exceptional mechanical strength due to their repetitive peptide motifs, which facilitate strong intermolecular interactions.[261] These properties make them well-suited for applications such as bone tissue engineering, where scaffolds must withstand mechanical forces. Elastin-like polypeptides, on the other hand, are widely used for soft tissue scaffolds such as skin and vascular scaffolds, owing to their excellent biocompatibility, low immunogenicity, and bioactive properties.[250,262] In tissue engineering, scaffolds must not only provide mechanical support but also mimic the extracellular matrix to promote cell adhesion, proliferation, and differentiation.[263] Peptide coacervates offer a unique advantage in this regard due to their structural resemblance to the extracellular matrix. This enables them to provide a supportive environment conducive to cell growth and tissue regeneration. Furthermore, the properties of coacervates can be tailored to meet the specific requirements of different tissues. For example, the mechanical strength and degradation rate of coacervate-based scaffolds can be adjusted to optimize them for bone, cartilage, or soft tissue applications. This customization is achieved by modifying the peptide sequences or coacervation conditions, enabling scaffolds to degrade at rates matching the regeneration needs of different tissues.[247,264] Integrating peptide coacervates into composite materials provides an opportunity to create hybrid scaffolds that combine the mechanical stability of synthetic polymers with the biological activity and tunability of peptides.[247] These hybrid systems retain the strength of traditional biomaterials while incorporating bioactive components that support tissue regeneration. Such composites enable the development of scaffolds that can endure mechanical forces yet offer the biochemical cues essential for tissue repair, making them suitable for applications in bone and cartilage engineering where both mechanical strength and biological responsiveness are required.

Despite the promising applications of peptide coacervates in tissue engineering and biomaterials, challenges remain in optimizing their properties for clinical use. One of the main challenges is achieving precise control over the coacervation process to ensure reproducibility and consistency in material properties. Variations in coacervate formation can lead to inconsistencies in scaffold performance, which could impact their effectiveness in clinical applications. Additionally, the long-term stability and biocompatibility of peptide-based materials must be carefully evaluated to ensure their suitability for *in vivo* use. These materials must degrade at a rate that matches tissue regeneration, and their degradation products must be non-toxic and biocompatible. Future research should focus on improving the design and functionality of peptide coacervates for specific tissue engineering applications. This includes exploring novel peptide sequences that enhance mechanical strength, environmental responsiveness, and bioactivity. Integrating peptide coacervates with other biomaterials, such as hydrogels or bioactive ceramics, may yield hybrid systems with enhanced performance, offering multifunctionality for applications across different tissue types.

5.2. Drug delivery systems

Peptide coacervates have emerged as a transformative platform for drug delivery, offering unique advantages over traditional systems like liposomes, polymers, and lipid nanoparticles.[265–270] While lipid-based carriers offer high biocompatibility and versatile drug encapsulation, they often suffer from low drug loading and require complex surface modification to address stability issues, endosomal entrapment, and high hepatic or splenic uptake.[268,271] Similarly, polymers face challenges such as particle aggregation and potential toxicity.[268] Peptide coacervates may overcome these hurdles through LLPS, producing micrometer-sized, membraneless droplets capable of sequestering a wide range of therapeutic molecules, including proteins, nucleic acids, and small molecules.[64,272,273] Encapsulation relies on non-covalent interactions, including electrostatic forces, hydrogen bonding, and hydrophobic interactions.[266] These interactions are crucial for maintaining the integrity and efficacy of therapeutic agents, particularly sensitive biomolecules like proteins and nucleic acids, which are susceptible to degradation in the biological environment.[62,239] By creating a stable microenvironment, peptide coacervates effectively shield therapeutic agents from premature degradation, ensuring that they reach their target site intact. Additionally, the amino acid-based composition allows for simple, precise tuning of physicochemical properties through single amino acid mutations, providing unparalleled adaptability and scalability compared to the labor-intensive fabrication of liposomes and polymers.[162] Furthermore, peptide coacervates exhibit negligible cytotoxicity and excellent biocompatibility, avoiding the safety concerns associated with inorganic nanoparticles and synthetic polymers.[258]

A defining feature of peptide coacervates-based drug delivery systems is their capacity for controlled and stimuli-responsive release of encapsulated therapeutics.[61,239,274] Redox-responsive peptide coacervates, for example, are designed to release their cargo in response to the redox conditions prevalent in specific physiological environments, such as the tumor microenvironment, which is often characterized by high levels of reducing agents.[62,239] This targeted release is particularly beneficial in cancer therapy, where minimizing systemic exposure and off-target effects is crucial. Wang *et al.* demonstrated that redox-responsive peptide coacervates could be engineered to selectively release tissue plasminogen activator in response to the reducing conditions found at thrombus sites, significantly enhancing the therapeutic efficacy and reducing off-target effects.[62] Similarly, another study by Sun *et al.* explored the potential of redox-responsive coacervates in the delivery of CRISPR-Cas9 complexes, where the coacervates disassembled in response to the intracellular reducing environment, allowing for efficient cytosolic delivery of the genome-editing tool.[239] These findings underscore the versatility of redox-responsive coacervates for site-specific drug delivery, making them a powerful platform for developing next-generation therapeutics. Fig. 10B illustrates the design of redox-responsive peptide coacervates, histidine-rich beak peptides conjugated with a lysine residue and a self-immolative moiety (HB*pep*-SR), that

can directly deliver a wide range of macromolecular therapeutics into the cytosols.[258] In a reducing environment, such as glutathione-rich cytosol, HB*pep*-SR is reduced, leading to self-catalytic cleavage of the SR moiety and disassembling of the coacervates. In addition to their redox-responsiveness, peptide coacervates also exhibit a high degree of modularity and adaptability, which can be leveraged to design sophisticated drug delivery systems. A notable aspect of this adaptability is the ability to encapsulate multiple substances within a single coacervate. Lim *et al.* developed glucose-responsive peptide coacervates that co-encapsulate insulin and glucose oxidase, providing a coordinated release of insulin in response to rising blood glucose levels.[64] This concept could extend other conditions, such as cancer or metabolic disorders, where multiple therapeutic targets require a coordinated response.[275,276] These multifunctional platforms enable the treatment of complex diseases through the simultaneous and responsive release of complementary drugs, potentially increasing treatment efficacy while minimizing side effects.

The interaction of peptide coacervates with biological membranes is another critical factor in their effectiveness as drug delivery systems.[277,278] Unlike traditional delivery vehicles that rely on lipid membranes, peptide coacervates can interact directly with the cytosol, facilitating efficient drug release inside cells. This is achieved through electrostatic attractions that promote cellular uptake *via* endocytosis or, in some cases, enable direct cytosolic delivery.[277] The work of Sun *et al.* exemplifies this potential by demonstrating the use of micrometer-sized peptide coacervates as delivery vesicles capable of crossing cell membranes without relying on endocytosis (Fig. 10B).[258] These coacervates, designed to be both pH- and redox-responsive, disassemble within the intracellular environment, releasing their cargo directly into the cytosol. This capability challenges the conventional belief that only nano-sized vesicles can penetrate cell membranes, suggesting that larger coacervates may also serve as effective delivery vehicles. This work highlighted the potential of peptide coacervates in delivering macromolecular therapeutics, including proteins, peptides, and RNAs, with both precision and efficiency, showcasing their utility in diverse therapeutic applications.

While peptide coacervates offer numerous advantages in drug delivery, challenges remain in translating them into clinical applications, primarily related to stability.[279] Without a traditional membrane, they are susceptible to a rapid coalescence or collapse in biological fluids.[280,281] Their stability is significantly influenced by environmental factors such as pH, temperature, and ionic strength.[56,190,219] For example, high ionic conditions can disrupt the interactions that maintain coacervate structure, causing premature release of encapsulated drugs.[219] Several strategies have been developed to address these challenges. One prominent approach is encasing coacervates within stabilizing membranes made of terpolymers, phospholipids, or polysaccharides.[282–284] These membranes can mitigate environmental sensitivity while retaining the ability to respond to external stimuli, although they may reduce permeability to large biomolecules. Cross-linking at the droplet interface is another effective approach.[63,285,286] The incorporation of stabilizing agents like polyphenols (*e.g.*, tannic acid) forms supramolecular networks, improving stability without compromising functionality.[63] Exposing coacervates to deionized water induces counterion extraction and physical crosslinking, resulting in the formation of viscoelastic interfaces that prevent fusion and enhance long-term stability.[286,287] Increasing the surface charge density, as indicated by high zeta potential, has also been reported to reduce droplet fusion through enhanced electrostatic repulsion.[153] Additionally, peptide coacervates have been stabilized against Ostwald ripening through a combination of attractive electrostatic interactions and translational entropy within the coacervates, where the charged nature of the components creates an energetic barrier that effectively suppresses droplet coarsening.[280] Beyond stability, another consideration is the potential immunogenicity of peptide coacervates, which must be carefully evaluated to avoid unwanted immune responses that could compromise their efficacy or safety.[288] Scalability of production is also a challenge, as consistent and reproducible manufacturing processes are essential for regulatory approval and clinical use. Advances in manufacturing techniques, including microfluidics and high-throughput screening offer promising solutions to streamline large-scale production.

Peptide coacervates represent a highly promising approach to drug delivery, offering controlled and targeted delivery of various therapeutic agents. Their ability to interact effectively with biological membranes, combined with customizability and multifunctionality, makes them a valuable tool in the development of next-generation drug delivery systems. As research in this field continues to advance, overcoming current challenges related to stability, immunogenicity, and scalability will be crucial to fully realizing the potential. Ongoing studies that delve into the mechanisms underlying coacervate formation, stability, and interaction with biological systems will be essential in advancing this field. The pioneering work on direct cytosolic delivery by micrometer-sized coacervates without endocytosis underscores the transformative potential of these systems, particularly for challenging applications such as cancer therapy and the delivery of macromolecular drugs.[258] Continued exploration in these areas will drive the transition of peptide coacervate-based systems from laboratory research to clinical applications, offering innovative solutions for treating complex diseases.

5.3. Synthetic biology

The concept of artificial cells, or protocells, represents a key frontier in synthetic biology, where researchers aim to build cell-like systems capable of replicating essential functions of living organisms.[53,289–294] Peptide coacervates have emerged as a promising platform for constructing these artificial cells due to their ability to create membraneless compartments that closely resemble the internal organization of natural cells.[53,295–297] This section examines the various roles of peptide coacervates in artificial cell development, emphasizing their role in mimicking cellular functions, supporting biochemical processes, and enabling complex synthetic biology applications.

One of the fundamental features of living cells is their compartmentalization, which allows for the segregation of biochemical processes and the establishment of specialized microenvironments. Peptide coacervates inherently possess the ability to form discrete, membraneless compartments, making them ideal candidates for constructing artificial cells.[53] These coacervates can encapsulate diverse biomolecules, such as nucleic acids, enzymes, and metabolites, thereby creating microenvironments that facilitate specific biochemical reactions.[298–300] The selective permeability of coacervate droplets is another critical attribute that mirrors the behavior of natural cellular membranes.[285] Coacervates can selectively sequester or exclude certain molecules based on their size, charge, or hydrophobicity. This property enables the coacervates to function as primitive organelles, where they can concentrate substrates, protect sensitive molecules, or control the flow of ions and other small molecules. Such selective permeability is crucial for maintaining the internal environment of artificial cells and ensuring that the encapsulated biochemical processes proceed efficiently.[65]

While coacervates naturally form membraneless compartments, they can also be integrated with structured membranes to create hybrid systems.[259,294,301] In these hybrid constructs, coacervates function as primitive organelles within structured membranes, providing localized environments for specific reactions, while the membranes not only prevent aggregation and coalescence but also regulate the selective biomolecule sequestration and chemical exchange across the membrane.[284] Fig. 10C illustrates hybrid PC@MPN protocells, where peptide coacervates (PCs), mimicking the cytosol, are coated with a metal-phenolic network (MPN) membrane.[259] The PCs are formed by the self-assembly of oppositely charged oligopeptides (R10 and D10), while the MPN membrane is generated through coordination between metal ions (*e.g.*, Fe^{3+}) and polyphenols (*e.g.*, tannic acid). This hybrid design provides structural stability while preserving the dynamic properties of coacervates, enabling the construction of artificial cells that can selectively exchange molecules and maintain internal biochemical processes. Furthermore, the integration of coacervates with structured membranes also enables the construction of more sophisticated artificial cells that can interact with their environment in a controlled manner.[302] Coacervate-membrane hybrids can be engineered to respond to changes in pH, temperature, or the presence of specific molecules, triggering the release of encapsulated contents or a change in the physical properties of the cell.[53,303,304]

The high degree of macromolecular crowding within coacervates mimics the crowded interior of living cells, which is known to significantly influence the kinetics and thermodynamics of biochemical reactions.[305] This crowded environment enhances the binding affinity between enzymes and substrates, accelerates reaction rates, and can stabilize proteins that would otherwise be unstable in dilute solutions.[300,306,307] One of the most striking demonstrations of the ability of coacervates to support biochemical reactions is their use in gene expression systems.[298] Coacervates have been shown to significantly enhance the transcription rates of genes, with rates that are comparable to those observed *in vivo*.[298] This enhancement is largely due to the increased binding constant of DNA to transcription factors and RNA polymerase in the crowded environment of the coacervate. The coacervate droplets can thus function as efficient microreactors for gene expression, supporting both transcription and translation within a confined space. Furthermore, coacervates have been used to construct artificial cells that can carry out more complex functions, such as the synthesis of proteins from DNA templates.[298,308,309] These artificial cells can encapsulate the entire transcription and translation machinery, enabling the production of functional proteins within the coacervate droplets. The ability to carry out such complex biochemical processes within coacervates highlights their potential as building blocks for more advanced synthetic cells.

Beyond simply supporting biochemical reactions, peptide coacervates can be engineered to simulate specific cellular processes, making them valuable for studying cellular dynamics and creating functional synthetic systems. Coacervates have been used to replicate aspects of cellular metabolism, such as the compartmentalization of metabolic pathways.[230,305,310] By confining different enzymes in separate coacervate droplets, it is possible to establish synthetic metabolic networks that carry out sequential reactions in a controlled manner. Fig. 10C demonstrates the capability of PC@MPN protocells to compartmentalize and sustain enzymatic cascade reactions. These protocells are loaded with enzymes such as glucose oxidase (GOx) and horseradish peroxidase (HRP), as well as the substrate Amplex Red (AR).[259] GOx catalyzes the oxidation of glucose to produce H_2O_2, which acts as a substrate for HRP to convert AR into resorufin (RS). The bright-field and fluorescence microscopy images confirm the success of this reaction, with red fluorescence indicating the production of RS. This example highlights how peptide coacervates can serve as compartments for synthetic metabolic networks, enabling sequential reactions within confined spaces. In addition to metabolic processes, coacervates have been used to model the dynamics of intracellular organelles.[295] Their liquid-like nature of coacervates allows them to undergo fusion and fission, similar to the behavior of natural membraneless organelles such as P granules.[36] This dynamic behavior can be harnessed to create artificial cells with controllable internal organization, where the distribution and interaction of coacervate-based organelles can be modulated in response to external stimuli.[100,296,311,312] Another key cellular process that can be mimicked using peptide coacervates is the assembly of nucleic acids and proteins into functional complexes.[300] By engineering coacervates to selectively encapsulate specific proteins and nucleic acids, it is possible to recreate these types of structures within artificial cells. This capability opens new avenues for studying the principles of cellular organization and for designing synthetic cells with custom-built compartments.

The unique properties of peptide coacervates make them highly suitable for various applications in biotechnology, particularly in the development of cell-free systems and biosensors.[313,314]

In cell-free protein synthesis, for example, coacervates can be used to create microreactors that enable the efficient production of proteins without requiring living cells. By creating optimized conditions within coacervates, these systems can be tailored to produce specific proteins or to screen gene expression constructs in high-throughput applications.[298,315] In biosensing, coacervate can encapsulate enzymes or other reactive molecules, forming droplets that respond to target analytes with high sensitivity. These biosensors can be used in a variety of applications, including medical diagnostics, environmental monitoring, and industrial process control.

Peptide coacervates offer a powerful and versatile platform for the construction of artificial cells. Their ability to mimic cellular compartmentalization, support complex biochemical reactions, and simulate dynamic cellular processes makes them invaluable for designing responsive and functional synthetic systems. By integrating coacervates with lipid membranes and other materials, sophisticated artificial cells could be created to interact dynamically with their environment and perform a wide range of functions.

6. Conclusions

Peptide-mediated liquid–liquid phase separation (LLPS) represents a rapidly evolving area of research with profound implications for both fundamental biology and applied sciences. Through this review, we have explored the intricate molecular mechanisms driving LLPS, the critical role of environmental factors in modulating phase behavior, and the diverse material properties of peptide coacervates. These insights highlight the versatility of LLPS as a mechanism for cellular organization and its potential for innovative applications in biotechnology and medicine. The dynamic nature of LLPS allows cells to compartmentalize and regulate biochemical processes without the need for traditional membrane-bound organelles, offering a flexible means of adapting to changing environmental conditions. This adaptability, however, also underscores the potential for dysregulation, which can lead to pathological states, including neurodegenerative diseases and cancer. Understanding the factors that govern the transition between liquid-like and solid-like states in biomolecular condensates is crucial for developing therapeutic strategies to mitigate these diseases. From a practical perspective, the ability to engineer peptide coacervates with tailored properties opens new avenues for applications in drug delivery, tissue engineering, and synthetic biology. The modularity and responsiveness of these systems to environmental stimuli make them ideal candidates for developing next-generation biomaterials and therapeutic platforms. However, challenges remain in ensuring the stability, biocompatibility, and scalability of peptide coacervates, which are essential for translating these promising technologies into clinical applications. In conclusion, LLPS is a powerful and versatile mechanism with significant potential to advance our understanding of cellular biology and to drive innovation in various scientific and medical fields. Continued research in this area will likely yield further breakthroughs, enabling the development of novel materials and therapeutic strategies that leverage the unique properties of glassy structures.[316–318]

Author contributions

Guangle Li: conceptualization, funding acquisition, investigation, writing – original draft, writing – review & editing; Chengqian Yuan: conceptualization, funding acquisition, writing – review & editing; Xuehai Yan: conceptualization, funding acquisition, project administration, writing – review & editing.

Data availability

The data supporting this article have been included as part of the ESI.†

Conflicts of interest

The authors declare no competing interests.

Acknowledgements

References

1 A. Ianiro, H. Wu, M. M. J. van Rijt, M. P. Vena, A. D. A. Keizer, A. C. C. Esteves, R. Tuinier, H. Friedrich, N. A. J. M. Sommerdijk and J. P. Patterson, *Nat. Chem.*, 2019, **11**, 320–328.

2 S. Alberti, A. Gladfelter and T. Mittag, *Cell*, 2019, **176**, 419–434.

3 D. Bracha, M. T. Walls, M.-T. Wei, L. Zhu, M. Kurian, J. L. Avalos, J. E. Toettcher and C. P. Brangwynne, *Cell*, 2018, **175**, 1467–1480.

4 F. Wang, P. Altschuh, L. Ratke, H. Zhang, M. Selzer and B. Nestler, *Adv. Mater.*, 2019, **31**, 1806733.

5 S. F. Banani, H. O. Lee, A. A. Hyman and M. K. Rosen, *Nat. Rev. Mol. Cell Biol.*, 2017, **18**, 285–298.

6 Y. Shin and C. P. Brangwynne, *Science*, 2017, **357**, eaaf4382.

7 S. Alberti and D. Dormann, *Annu. Rev. Genet.*, 2019, **53**, 171–194.

8 E. Gomes and J. Shorter, *J. Biol. Chem.*, 2019, **294**, 7115–7127.

9 Timothy J. Nott, E. Petsalaki, P. Farber, D. Jervis, E. Fussner, A. Plochowietz, T. D. Craggs, David P. Bazett-

Jones, T. Pawson, Julie D. Forman-Kay and Andrew J. Baldwin, *Mol. Cell*, 2015, **57**, 936–947.

10 Y. Dai, L. You and A. Chilkoti, *Nat. Rev. Bioeng.*, 2023, **1**, 466–480.

11 T. Hirose, K. Ninomiya, S. Nakagawa and T. Yamazaki, *Nat. Rev. Mol. Cell Biol.*, 2023, **24**, 288–304.

12 Y. Dai, Z. Zhou, W. Yu, Y. Ma, K. Kim, N. Rivera, J. Mohammed, E. Lantelme, H. Hsu-Kim, A. Chilkoti and L. You, *Cell*, 2024, **187**, 5951–5966.

13 X. Su, J. A. Ditlev, E. Hui, W. Xing, S. Banjade, J. Okrut, D. S. King, J. Taunton, M. K. Rosen and R. D. Vale, *Science*, 2016, **352**, 595–599.

14 A. R. Strom, A. V. Emelyanov, M. Mir, D. V. Fyodorov, X. Darzacq and G. H. Karpen, *Nature*, 2017, **547**, 241–245.

15 C. Roden and A. S. Gladfelter, *Nat. Rev. Mol. Cell Biol.*, 2021, **22**, 183–195.

16 M.-T. Wei, Y.-C. Chang, S. F. Shimobayashi, Y. Shin, A. R. Strom and C. P. Brangwynne, *Nat. Cell Biol.*, 2020, **22**, 1187–1196.

17 J. A. Riback, C. D. Katanski, J. L. Kear-Scott, E. V. Pilipenko, A. E. Rojek, T. R. Sosnick and D. A. Drummond, *Cell*, 2017, **168**, 1028–1040.

18 N. N. Noda, Z. Wang and H. Zhang, *J. Cell Biol.*, 2020, **219**, e202004062.

19 A. S. Lyon, W. B. Peeples and M. K. Rosen, *Nat. Rev. Mol. Cell Biol.*, 2021, **22**, 215–235.

20 X. Wu, Q. Cai, Z. Feng and M. Zhang, *Dev. Cell*, 2020, **55**, 18–29.

21 J. Y. Ong and J. Z. Torres, *Mol. Cell*, 2020, **80**, 9–20.

22 B. Wang, L. Zhang, T. Dai, Z. Qin, H. Lu, L. Zhang and F. Zhou, *Signal Transduction Targeted Ther.*, 2021, **6**, 290.

23 E. Astoricchio, C. Alfano, L. Rajendran, P. A. Temussi and A. Pastore, *Trends Biochem. Sci.*, 2020, **45**, 706–717.

24 S. Mehta and J. Zhang, *Nat. Rev. Cancer*, 2022, **22**, 239–252.

25 S. Yang, W. Shen, J. Hu, S. Cai, C. Zhang, S. Jin, X. Guan, J. Wu, Y. Wu and J. Cui, *Front. Immunol.*, 2023, **14**, 1162211.

26 G. Pei, H. Lyons, P. Li and B. R. Sabari, *Nat. Rev. Mol. Cell Biol.*, 2024, DOI: **10.1038/s41580-024-00789-x**.

27 S. Elbaum-Garfinkle, *J. Biol. Chem.*, 2019, **294**, 7160–7168.

28 B. S. Visser, W. P. Lipiński and E. Spruijt, *Nat. Rev. Chem.*, 2024, **8**, 686–700.

29 S. Wang, T. Dai, Z. Qin, T. Pan, F. Chu, L. Lou, L. Zhang, B. Yang, H. Huang, H. Lu and F. Zhou, *Nat. Cell Biol.*, 2021, **23**, 718–732.

30 T. Liang, Y. Dong, I. Cheng, P. Wen, F. Li, F. Liu, Q. Wu, E. Ren, P. Liu, H. Li and Z. Gu, *Nat. Biomed. Eng.*, 2024, **8**, 1469–1482.

31 Z. Wang and H. Zhang, *Trends Cell Biol.*, 2019, **29**, 417–427.

32 Z.-G. Qian, S.-C. Huang and X.-X. Xia, *Nat. Chem. Biol.*, 2022, **18**, 1330–1340.

33 R. K. Das, K. M. Ruff and R. V. Pappu, *Curr. Opin. Struct. Biol.*, 2015, **32**, 102–112.

34 T. S. Harmon, A. S. Holehouse, M. K. Rosen and R. V. Pappu, *eLife*, 2017, **6**, e30294.

35 J. Wang, J.-M. Choi, A. S. Holehouse, H. O. Lee, X. Zhang, M. Jahnel, S. Maharana, R. Lemaitre, A. Pozniakovsky,

D. Drechsel, I. Poser, R. V. Pappu, S. Alberti and A. A. Hyman, *Cell*, 2018, **174**, 688–699.

36 C. P. Brangwynne, C. R. Eckmann, D. S. Courson, A. Rybarska, C. Hoege, J. Gharakhani, F. Jülicher and A. A. Hyman, *Science*, 2009, **324**, 1729–1732.

37 S. F. Banani, A. M. Rice, W. B. Peeples, Y. Lin, S. Jain, R. Parker and M. K. Rosen, *Cell*, 2016, **166**, 651–663.

38 Y. Lin, David S. W. Protter, Michael K. Rosen and R. Parker, *Mol. Cell*, 2015, **60**, 208–219.

39 P. Li, S. Banjade, H.-C. Cheng, S. Kim, B. Chen, L. Guo, M. Llaguno, J. V. Hollingsworth, D. S. King, S. F. Banani, P. S. Russo, Q.-X. Jiang, B. T. Nixon and M. K. Rosen, *Nature*, 2012, **483**, 336–340.

40 D. L. J. Lafontaine, J. A. Riback, R. Bascetin and C. P. Brangwynne, *Nat. Rev. Mol. Cell Biol.*, 2021, **22**, 165–182.

41 C. P. Brangwynne, T. J. Mitchison and A. A. Hyman, *Proc. Natl. Acad. Sci. U. S. A.*, 2011, **108**, 4334–4339.

42 D. S. W. Protter and R. Parker, *Trends Cell Biol.*, 2016, **26**, 668–679.

43 B. Van Treeck, D. S. W. Protter, T. Matheny, A. Khong, C. D. Link and R. Parker, *Proc. Natl. Acad. Sci. U. S. A.*, 2018, **115**, 2734–2739.

44 Q. Wang, I. A. Sawyer, M.-H. Sung, D. Sturgill, S. P. Shevtsov, G. Pegoraro, O. Hakim, S. Baek, G. L. Hager and M. Dundr, *Nat. Commun.*, 2016, **7**, 10966.

45 J. L. Watson, E. Seinkmane, C. T. Styles, A. Mihut, L. K. Krüger, K. E. McNally, V. J. Planelles-Herrero, M. Dudek, P. M. McCall, S. Barbiero, M. Vanden Oever, S. Y. Peak-Chew, B. T. Porebski, A. Zeng, N. M. Rzechorzek, D. C. S. Wong, A. D. Beale, A. Stangherlin, M. Riggi, J. Iwasa, J. Morf, C. Miliotis, A. Guna, A. J. Inglis, J. Brugués, R. M. Voorhees, J. E. Chambers, Q.-J. Meng, J. S. O'Neill, R. S. Edgar and E. Derivery, *Nature*, 2023, **623**, 842–852.

46 Z. Gao, W. Zhang, R. Chang, S. Zhang, G. Yang and G. Zhao, *Front. Microbiol.*, 2021, **12**, 751880.

47 S. Boeynaems, S. Alberti, N. L. Fawzi, T. Mittag, M. Polymenidou, F. Rousseau, J. Schymkowitz, J. Shorter, B. Wolozin, L. Van Den Bosch, P. Tompa and M. Fuxreiter, *Trends Cell Biol.*, 2018, **28**, 420–435.

48 A. Boija, I. A. Klein, B. R. Sabari, A. Dall'Agnese, E. L. Coffey, A. V. Zamudio, C. H. Li, K. Shrinivas, J. C. Manteiga, N. M. Hannett, B. J. Abraham, L. K. Afeyan, Y. E. Guo, J. K. Rimel, C. B. Fant, J. Schuijers, T. I. Lee, D. J. Taatjes and R. A. Young, *Cell*, 2018, **175**, 1842–1855.

49 S. Alberti and A. A. Hyman, *Nat. Rev. Mol. Cell Biol.*, 2021, **22**, 196–213.

50 K. Jaqaman and J. A. Ditlev, *Curr. Opin. Cell Biol.*, 2021, **69**, 48–54.

51 C. Yuan, Q. Li, R. Xing, J. Li and X. Yan, *Chem*, 2023, **9**, 2425–2445.

52 A. Lampel, *Chem*, 2020, **6**, 1222–1236.

53 M. Abbas, W. P. Lipiński, J. Wang and E. Spruijt, *Chem. Soc. Rev.*, 2021, **50**, 3690–3705.

54 S. Song, T. Ivanov, D. Yuan, J. Wang, L. C. da Silva, J. Xie and S. Cao, *Biomacromolecules*, 2024, **25**, 5468–5488.

55 M. Naz, L. Zhang, C. Chen, S. Yang, H. Dou, S. Mann and J. Li, *Commun. Chem.*, 2024, **7**, 79.

56 A. Sathyavageeswaran, J. Bonesso Sabadini and S. L. Perry, *Acc. Chem. Res.*, 2024, **57**, 386–398.

57 A. Baruch Leshem, S. Sloan-Dennison, T. Massarano, S. Ben-David, D. Graham, K. Faulds, H. E. Gottlieb, J. H. Chill and A. Lampel, *Nat. Commun.*, 2023, **14**, 421.

58 D. Priftis, L. Leon, Z. Song, S. L. Perry, K. O. Margossian, A. Tropnikova, J. Cheng and M. Tirrell, *Angew. Chem., Int. Ed.*, 2015, **54**, 11128–11132.

59 L. Ma, X. Fang and C. Wang, *Front. Bioeng. Biotechnol.*, 2023, **10**, 1100365.

60 R. Augustine, N. Kalva, H. A. Kim, Y. Zhang and I. Kim, *Molecules*, 2019, **24**, 2961.

61 J. D. Tang, S. R. Caliari and K. J. Lampe, *Biomacromolecules*, 2018, **19**, 3925–3935.

62 J. Wang, M. Abbas, Y. Huang, J. Wang and Y. Li, *Commun. Chem.*, 2023, **6**, 243.

63 W. Yim, Z. Jin, Y.-C. Chang, C. Brambila, M. N. Creyer, C. Ling, T. He, Y. Li, M. Retout, W. F. Penny, J. Zhou and J. V. Jokerst, *Nat. Commun.*, 2024, **15**, 7295.

64 Z. W. Lim, Y. Ping and A. Miserez, *Bioconjugate Chem.*, 2018, **29**, 2176–2180.

65 S. Cao, T. Ivanov, J. Heuer, C. T. J. Ferguson, K. Landfester and L. Caire da Silva, *Nat. Commun.*, 2024, **15**, 39.

66 H. Betre, L. A. Setton, D. E. Meyer and A. Chilkoti, *Biomacromolecules*, 2002, **3**, 910–916.

67 J. Sun, L. Xiao, B. Li, K. Zhao, Z. Wang, Y. Zhou, C. Ma, J. Li, H. Zhang, A. Herrmann and K. Liu, *Angew. Chem., Int. Ed.*, 2021, **60**, 23687–23694.

68 S. Koga, D. S. Williams, A. W. Perriman and S. Mann, *Nat. Chem.*, 2011, **3**, 720–724.

69 E. W. Martin and T. Mittag, *Biochemistry*, 2018, **57**, 2478–2487.

70 S. Mukherjee and L. V. Schäfer, *Nat. Commun.*, 2023, **14**, 5892.

71 M. L. Huggins, *J. Phys. Chem.*, 1942, **46**, 151–158.

72 P. J. Flory, *J. Chem. Phys.*, 1942, **10**, 51–61.

73 J. T. G. Overbeek and M. J. Voorn, *J. Cell. Comp. Physiol.*, 1957, **49**, 7–26.

74 X. Wei, J. Zhou, Y. Wang and F. Meng, *Phys. Rev. Lett.*, 2020, **125**, 268001.

75 A. C. Murthy, G. L. Dignon, Y. Kan, G. H. Zerze, S. H. Parekh, J. Mittal and N. L. Fawzi, *Nat. Struct. Mol. Biol.*, 2019, **26**, 637–648.

76 M.-T. Wei, S. Elbaum-Garfinkle, A. S. Holehouse, C. C.-H. Chen, M. Feric, C. B. Arnold, R. D. Priestley, R. V. Pappu and C. P. Brangwynne, *Nat. Chem.*, 2017, **9**, 1118–1125.

77 A. Gobbi and G. Frenking, *J. Am. Chem. Soc.*, 1993, **115**, 2362–2372.

78 B. Gabryelczyk, H. Cai, X. Shi, Y. Sun, P. J. M. Swinkels, S. Salentinig, K. Pervushin and A. Miserez, *Nat. Commun.*, 2019, **10**, 5465.

79 Q. Guo, G. Zou, X. Qian, S. Chen, H. Gao and J. Yu, *Nat. Commun.*, 2022, **13**, 5771.

80 W. Wei, Y. Tan, N. R. Martinez Rodriguez, J. Yu, J. N. Israelachvili and J. H. Waite, *Acta Biomater.*, 2014, **10**, 1663–1670.

81 Y. Hong, S. Najafi, T. Casey, J.-E. Shea, S.-I. Han and D. S. Hwang, *Nat. Commun.*, 2022, **13**, 7326.

82 X. Wu, Y. Sun, J. Yu and A. Miserez, *Commun. Chem.*, 2024, **7**, 5.

83 K. Deepankumar, Q. Guo, H. Mohanram, J. Lim, Y. Mu, K. Pervushin, J. Yu and A. Miserez, *Adv. Mater.*, 2022, **34**, 2103828.

84 V. Castelletto, J. Seitsonen, A. Pollitt and I. W. Hamley, *Biomacromolecules*, 2024, **25**, 5321–5331.

85 D. A. Dougherty, *Science*, 1996, **271**, 163–168.

86 X. Ren, Q. Zou, C. Yuan, R. Chang, R. Xing and X. Yan, *Angew. Chem., Int. Ed.*, 2019, **58**, 5872–5876.

87 D. Su, Y. Yu, L. Zhao, T. Wang and X. Yan, *Acta Chim. Sin.*, 2023, **81**, 1486–1492.

88 S. Qamar, G. Wang, S. J. Randle, F. S. Ruggeri, J. A. Varela, J. Q. Lin, E. C. Phillips, A. Miyashita, D. Williams, F. Ströhl, W. Meadows, R. Ferry, V. J. Dardov, G. G. Tartaglia, L. A. Farrer, G. S. Kaminski Schierle, C. F. Kaminski, C. E. Holt, P. E. Fraser, G. Schmitt-Ulms, D. Klenerman, T. Knowles, M. Vendruscolo and P. St George-Hyslop, *Cell*, 2018, **173**, 720–734.

89 S. Rekhi, C. G. Garcia, M. Barai, A. Rizuan, B. S. Schuster, K. L. Kiick and J. Mittal, *Nat. Chem.*, 2024, **16**, 1113–1124.

90 I. Katzir, E. Haimov and A. Lampel, *Adv. Mater.*, 2022, **34**, 2206371.

91 Chi W. Pak, M. Kosno, Alex S. Holehouse, Shae B. Padrick, A. Mittal, R. Ali, Ali A. Yunus, David R. Liu, Rohit V. Pappu and Michael K. Rosen, *Mol. Cell*, 2016, **63**, 72–85.

92 Y. Lin, S. L. Currie and M. K. Rosen, *J. Biol. Chem.*, 2017, **292**, 19110–19120.

93 E. W. Martin and A. S. Holehouse, *Emerging Top. Life Sci.*, 2020, **4**, 307–329.

94 F. G. Quiroz and A. Chilkoti, *Nat. Mater.*, 2015, **14**, 1164–1171.

95 E. W. Martin, A. S. Holehouse, I. Peran, M. Farag, J. J. Incicco, A. Bremer, C. R. Grace, A. Soranno, R. V. Pappu and T. Mittag, *Science*, 2020, **367**, 694–699.

96 B. S. Schuster, G. L. Dignon, W. S. Tang, F. M. Kelley, A. K. Ranganath, C. N. Jahnke, A. G. Simpkins, R. M. Regy, D. A. Hammer, M. C. Good and J. Mittal, *Proc. Natl. Acad. Sci. U. S. A.*, 2020, **117**, 11421–11431.

97 A. Bremer, M. Farag, W. M. Borcherds, I. Peran, E. W. Martin, R. V. Pappu and T. Mittag, *Nat. Chem.*, 2022, **14**, 196–207.

98 A. Netzer, A. Baruch Leshem, S. Veretnik, I. Edelstein and A. Lampel, *Small*, 2024, **20**, 2401665.

99 Y. Tang, S. Bera, Y. Yao, J. Zeng, Z. Lao, X. Dong, E. Gazit and G. Wei, *Cell Rep. Phys. Sci.*, 2021, **2**, 100579.

100 R. Kubota, S. Torigoe and I. Hamachi, *J. Am. Chem. Soc.*, 2022, **144**, 15155–15164.

101 D. Sementa, D. Dave, R. S. Fisher, T. Wang, S. Elbaum-Garfinkle and R. V. Ulijn, *Angew. Chem., Int. Ed.*, 2023, **62**, e202311479.

102 K. W. Y. Chan, M. Navi, J. Kieda, T. Moran, D. Hammers, S. Lee and S. S. H. Tsai, *Lab Chip*, 2022, **22**, 2647–2656.

103 N. O. Taylor, M.-T. Wei, H. A. Stone and C. P. Brangwynne, *Biophys. J.*, 2019, **117**, 1285–1300.

104 A. Molliex, J. Temirov, J. Lee, M. Coughlin, A. P. Kanagaraj, H. J. Kim, T. Mittag and J. P. Taylor, *Cell*, 2015, **163**, 123–133.

105 S. Elbaum-Garfinkle, Y. Kim, K. Szczepaniak, C. C.-H. Chen, C. R. Eckmann, S. Myong and C. P. Brangwynne, *Proc. Natl. Acad. Sci. U. S. A.*, 2015, **112**, 7189–7194.

106 A. Patel, Hyun O. Lee, L. Jawerth, S. Maharana, M. Jahnel, Marco Y. Hein, S. Stoynov, J. Mahamid, S. Saha, Titus M. Franzmann, A. Pozniakovski, I. Poser, N. Maghelli, Loic A. Royer, M. Weigert, Eugene W. Myers, S. Grill, D. Drechsel, Anthony A. Hyman and S. Alberti, *Cell*, 2015, **162**, 1066–1077.

107 I. Alshareedah, T. Kaur, J. Ngo, H. Seppala, L.-A. D. Kounatse, W. Wang, M. M. Moosa and P. R. Banerjee, *J. Am. Chem. Soc.*, 2019, **141**, 14593–14602.

108 P. R. Banerjee, A. N. Milin, M. M. Moosa, P. L. Onuchic and A. A. Deniz, *Angew. Chem., Int. Ed.*, 2017, **56**, 11354–11359.

109 M. Feric, N. Vaidya, T. S. Harmon, D. M. Mitrea, L. Zhu, T. M. Richardson, R. W. Kriwacki, R. V. Pappu and C. P. Brangwynne, *Cell*, 2016, **165**, 1686–1697.

110 S. Jain, Joshua R. Wheeler, Robert W. Walters, A. Agrawal, A. Barsic and R. Parker, *Cell*, 2016, **164**, 487–498.

111 N. Galvanetto, M. T. Ivanović, A. Chowdhury, A. Sottini, M. F. Nüesch, D. Nettels, R. B. Best and B. Schuler, *Nature*, 2023, **619**, 876–883.

112 H. Le Ferrand, M. Duchamp, B. Gabryelczyk, H. Cai and A. Miserez, *J. Am. Chem. Soc.*, 2019, **141**, 7202–7210.

113 S. Guseva, V. Schnapka, W. Adamski, D. Maurin, R. W. H. Ruigrok, N. Salvi and M. Blackledge, *J. Am. Chem. Soc.*, 2023, **145**, 10548–10563.

114 W. E. Arter, R. Qi, N. A. Erkamp, G. Krainer, K. Didi, T. J. Welsh, J. Acker, J. Nixon-Abell, S. Qamar, J. Guillén-Boixet, T. M. Franzmann, D. Kuster, A. A. Hyman, A. Borodavka, P. S. George-Hyslop, S. Alberti and T. P. J. Knowles, *Nat. Commun.*, 2022, **13**, 7845.

115 I. Alshareedah, T. Kaur and P. R. Banerjee, in *Methods in Enzymology*, ed. C. D. Keating, Academic Press, 2021, vol. 646, pp. 143–183.

116 I. Alshareedah, G. M. Thurston and P. R. Banerjee, *Biophys. J.*, 2021, **120**, 1161–1169.

117 R. S. Fisher and S. Elbaum-Garfinkle, *Nat. Commun.*, 2020, **11**, 4628.

118 X. Zhang, H. Li, Y. Ma, D. Zhong and S. Hou, *APL Bioeng.*, 2023, **7**, 021502.

119 S. Ambadipudi, J. Biernat, D. Riedel, E. Mandelkow and M. Zweckstetter, *Nat. Commun.*, 2017, **8**, 275.

120 N. M. Kanaan, C. Hamel, T. Grabinski and B. Combs, *Nat. Commun.*, 2020, **11**, 2809.

121 H. Zhang, S. Shao and Y. Sun, *Biophys. Rep.*, 2022, **8**, 2–13.

122 S. V. Ulianov, Artem K. Velichko, M. D. Magnitov, Artem V. Luzhin, A. K. Golov, N. Ovsyannikova, I. I. Kireev, Alexey S. Gavrikov, Alexander S. Mishin, A. K. Garaev, A. V. Tyakht, Alexey A. Gavrilov, O. L. Kantidze and S. V. Razin, *Nucleic Acids Res.*, 2021, **49**, 10524–10541.

123 K. A. Ibrahim, A. S. Naidu, H. Miljkovic, A. Radenovic and W. Yang, *ACS Nano*, 2024, **18**, 10738–10757.

124 G. Scarcelli and S. H. Yun, *Nat. Photonics*, 2008, **2**, 39–43.

125 R. Prevedel, A. Diz-Muñoz, G. Ruocco and G. Antonacci, *Nat. Methods*, 2019, **16**, 969–977.

126 R. Schlüßler, K. Kim, M. Nötzel, A. Taubenberger, S. Abuhattum, T. Beck, P. Müller, S. Maharana, G. Cojoc, S. Girardo, A. Hermann, S. Alberti and J. Guck, *eLife*, 2022, **11**, e68490.

127 G. Antonacci, V. de Turris, A. Rosa and G. Ruocco, *Commun. Biol.*, 2018, **1**, 139.

128 R. De Santis, V. Alfano, V. de Turris, A. Colantoni, L. Santini, M. G. Garone, G. Antonacci, G. Peruzzi, E. Sudria-Lopez, E. Wyler, J. J. Anink, E. Aronica, M. Landthaler, R. J. Pasterkamp, I. Bozzoni and A. Rosa, *Cell Rep.*, 2019, **27**, 3818–3831.

129 S. Kim, J. Huang, Y. Lee, S. Dutta, H. Y. Yoo, Y. M. Jung, Y. Jho, H. Zeng and D. S. Hwang, *Proc. Natl. Acad. Sci. U. S. A.*, 2016, **113**, E847–E853.

130 C. Yuan, A. Levin, W. Chen, R. Xing, Q. Zou, T. W. Herling, P. K. Challa, T. P. J. Knowles and X. Yan, *Angew. Chem., Int. Ed.*, 2019, **58**, 18116–18123.

131 J. E. Bramham and A. P. Golovanov, *Nat. Commun.*, 2022, **13**, 1767.

132 S. E. Reichheld, L. D. Muiznieks, F. W. Keeley and S. Sharpe, *Proc. Natl. Acad. Sci. U. S. A.*, 2017, **114**, E4408–E4415.

133 H. Cai, B. Gabryelczyk, M. S. S. Manimekalai, G. Grüber, S. Salentinig and A. Miserez, *Soft Matter*, 2017, **13**, 7740–7752.

134 S. Da Vela, M. K. Braun, A. Dörr, A. Greco, J. Möller, Z. Fu, F. Zhang and F. Schreiber, *Soft Matter*, 2016, **12**, 9334–9341.

135 N. Salvi, A. Abyzov and M. Blackledge, *Angew. Chem., Int. Ed.*, 2017, **56**, 14020–14024.

136 C. F. Pantoja, A. Ibáñez de Opakua, M.-S. Cima-Omori and M. Zweckstetter, *Angew. Chem., Int. Ed.*, 2023, **62**, e202218078.

137 T. H. Kim, B. J. Payliss, M. L. Nosella, I. T. W. Lee, Y. Toyama, J. D. Forman-Kay and L. E. Kay, *Proc. Natl. Acad. Sci. U. S. A.*, 2021, **118**, e2104897118.

138 E. W. Martin, T. S. Harmon, J. B. Hopkins, S. Chakravarthy, J. J. Incicco, P. Schuck, A. Soranno and T. Mittag, *Nat. Commun.*, 2021, **12**, 4513.

139 G. Bianchi, S. Longhi, R. Grandori and S. Brocca, *Int. J. Mol. Sci.*, 2020, **21**, 6208.

140 S. Maiti, A. Singh, T. Maji, N. V. Saibo and S. De, *Curr. Res. Struct. Biol.*, 2024, **7**, 100138.

141 O. Matsarskaia, S. Da Vela, A. Mariani, Z. Fu, F. Zhang and F. Schreiber, *J. Phys. Chem. B*, 2019, **123**, 1913–1919.

142 S. L. Burg, A. Washington, D. M. Coles, A. Bianco, D. McLoughlin, O. O. Mykhaylyk, J. Villanova, A. J. C. Dennison, C. J. Hill, P. Vukusic, S. Doak, S. J. Martin, M. Hutchings, S. R. Parnell, C. Vasilev, N. Clarke, A. J. Ryan, W. Furnass, M. Croucher, R. M. Dalgliesh, S. Prevost, R. Dattani, A. Parker, R. A. L. Jones, J. P. A. Fairclough and A. J. Parnell, *Commun. Chem.*, 2019, **2**, 100.

143 C. A. Brosey and J. A. Tainer, *Curr. Opin. Struct. Biol.*, 2019, **58**, 197–213.

144 N. A. Erkamp, R. Qi, T. J. Welsh and T. P. J. Knowles, *Lab Chip*, 2023, **23**, 9–24.

145 M. Linsenmeier, M. R. G. Kopp, S. Stavrakis, A. de Mello and P. Arosio, *Biochim. Biophys. Acta, Mol. Cell Res.*, 2021, **1868**, 118823.

146 T. Beneyton, C. Love, M. Girault, T.-Y. D. Tang and J.-C. Baret, *ChemSystemsChem*, 2020, **2**, e2000022.

147 M. Linsenmeier, M. R. G. Kopp, F. Grigolato, L. Emmanoulidis, D. Liu, D. Zürcher, M. Hondele, K. Weis, U. Capasso Palmiero and P. Arosio, *Angew. Chem., Int. Ed.*, 2019, **58**, 14489–14494.

148 M. R. G. Kopp, M. Linsenmeier, B. Hettich, S. Prantl, S. Stavrakis, J.-C. Leroux and P. Arosio, *Anal. Chem.*, 2020, **92**, 5803–5812.

149 A. Bremer, T. Mittag and M. Heymann, *Lab Chip*, 2020, **20**, 4225–4234.

150 L. Li, D. Mustafi, Q. Fu, V. Tereshko, D. L. Chen, J. D. Tice and R. F. Ismagilov, *Proc. Natl. Acad. Sci. U. S. A.*, 2006, **103**, 19243–19248.

151 P. Li, X. Zeng, S. Li, X. Xiang, P. Chen, Y. Li and B.-F. Liu, *Anal. Chem.*, 2022, **94**, 687–694.

152 Y. Shen, F. S. Ruggeri, D. Vigolo, A. Kamada, S. Qamar, A. Levin, C. Iserman, S. Alberti, P. S. George-Hyslop and T. P. J. Knowles, *Nat. Nanotechnol.*, 2020, **15**, 841–847.

153 T. J. Welsh, G. Krainer, J. R. Espinosa, J. A. Joseph, A. Sridhar, M. Jahnel, W. E. Arter, K. L. Saar, S. Alberti, R. Collepardo-Guevara and T. P. J. Knowles, *Nano Lett.*, 2022, **22**, 612–621.

154 N. Taylor, S. Elbaum-Garfinkle, N. Vaidya, H. Zhang, H. A. Stone and C. P. Brangwynne, *Soft Matter*, 2016, **12**, 9142–9150.

155 Q. Ma, Y. Song, W. Sun, J. Cao, H. Yuan, X. Wang, Y. Sun and H. C. Shum, *Adv. Sci.*, 2020, **7**, 1903359.

156 M. Tsanai, Pim W. J. M. Frederix, C. F. E. Schroer, P. C. T. Souza and S. J. Marrink, *Chem. Sci.*, 2021, **12**, 8521–8530.

157 X. Chu, T. Sun, Q. Li, Y. Xu, Z. Zhang, L. Lai and J. Pei, *BMC Bioinf.*, 2022, **23**, 72.

158 X. Yang, Y. Wang and G. Yang, *Sci. Rep.*, 2024, **14**, 13382.

159 H. Cai, R. M. Vernon and J. D. Forman-Kay, *Biomolecules*, 2022, **12**, 1131.

160 K. Yu, Z. Liu, H. Cheng, S. Li, Q. Zhang, J. Liu, H.-Q. Ju, Z. Zuo, Q. Zhao, S. Kang and Z.-X. Liu, *Briefings Bioinf.*, 2023, **24**, bbac550.

161 I. Kaminker, W. Wei, A. M. Schrader, Y. Talmon, M. T. Valentine, J. N. Israelachvili, J. H. Waite and S. Han, *Soft Matter*, 2017, **13**, 9122–9131.

162 S. H. Hiew, Y. Lu, H. Han, R. A. Gonçalves, S. R. Alfarano, R. Mezzenga, A. N. Parikh, Y. Mu and A. Miserez, *J. Am. Chem. Soc.*, 2023, **145**, 3382–3393.

163 H. Wang, F. M. Kelley, D. Milovanovic, B. S. Schuster and Z. Shi, *Biophys. Rep.*, 2021, **1**, 100011.

164 G. Li, X. Xu and Y. Y. Zuo, *J. Colloid Interface Sci.*, 2023, **630**, 21–27.

165 G. Li, X. Xu and Y. Y. Zuo, *Biophys. J.*, 2023, **122**, 1772–1780.

166 G. Li, X. Xu and Y. Y. Zuo, *Biophys. J.*, 2023, **122**, 3099–3107.

167 B. Gouveia, Y. Kim, J. W. Shaevitz, S. Petry, H. A. Stone and C. P. Brangwynne, *Nature*, 2022, **609**, 255–264.

168 Y. Sun, X. Wu, J. Li, M. Radiom, R. Mezzenga, C. S. Verma, J. Yu and A. Miserez, *Nat. Commun.*, 2024, **15**, 10094.

169 I. Alshareedah, A. Singh, S. Yang, V. Ramachandran, A. Quinn, D. A. Potoyan and P. R. Banerjee, *Sci. Adv.*, 2024, **10**, eadi6539.

170 R. S. Fisher and A. C. Obermeyer, *Chem. Sci.*, 2024, **15**, 19795–19804.

171 A. R. Strom, Y. Kim, H. Zhao, Y.-C. Chang, N. D. Orlovsky, A. Košmrlj, C. Storm and C. P. Brangwynne, *Cell*, 2024, **187**, 5282–5297.

172 L. Zhu, Y. Pan, Z. Hua, Y. Liu and X. Zhang, *J. Am. Chem. Soc.*, 2024, **146**, 14307–14317.

173 J. V. Roggeveen, H. Wang, Z. Shi and H. A. Stone, *Biophys. J.*, 2024, **123**, 1393–1403.

174 D. Sundaravadivelu Devarajan, J. Wang, B. Szała-Mendyk, S. Rekhi, A. Nikoubashman, Y. C. Kim and J. Mittal, *Nat. Commun.*, 2024, **15**, 1912.

175 Y. Wang, S. Li, M. Mokbel, A. I. May, Z. Liang, Y. Zeng, W. Wang, H. Zhang, F. Yu, K. Sporbeck, L. Jiang, S. Aland, J. Agudo-Canalejo, R. L. Knorr and X. Fang, *Nature*, 2024, **634**, 1204–1210.

176 L. D. Zarzar, V. Sresht, E. M. Sletten, J. A. Kalow, D. Blankschtein and T. M. Swager, *Nature*, 2015, **518**, 520–524.

177 J. Marthelot, E. F. Strong, P. M. Reis and P. T. Brun, *Nat. Commun.*, 2018, **9**, 4477.

178 E. Spruijt, J. Sprakel, M. A. Cohen Stuart and J. van der Gucht, *Soft Matter*, 2010, **6**, 172–178.

179 A. Mangiarotti, N. Chen, Z. Zhao, R. Lipowsky and R. Dimova, *Nat. Commun.*, 2023, **14**, 2809.

180 Y. Zhang, R. Prasad, S. Su, D. Lee and H.-X. Zhou, *Cell Rep. Phys. Sci.*, 2024, **5**, 102218.

181 A. Ghosh, D. Kota and H.-X. Zhou, *Nat. Commun.*, 2021, **12**, 5995.

182 F. K. Hansen, *J. Colloid Interface Sci.*, 1993, **160**, 209–217.

183 H. Cinar, Z. Fetahaj, S. Cinar, R. M. Vernon, H. S. Chan and R. H. A. Winter, *Chem. - Eur. J.*, 2019, **25**, 13049–13069.

184 S. Gudlur, F. V. Ferreira, J. S. M. Ting, C. Domene, S. Maricar, A. P. Le Brun, N. Yepuri, M. Moir, R. Russell, T. Darwish, A. Miserez and M. Cárdenas, *Front. Soft Matter*, 2024, **3**.

185 A. A. M. André and E. Spruijt, *Int. J. Mol. Sci.*, 2020, **21**, 5908.

186 S. S. Ribeiro, N. Samanta, S. Ebbinghaus and J. C. Marcos, *Nat. Rev. Chem.*, 2019, **3**, 552–561.

187 J. A. Villegas, M. Heidenreich and E. D. Levy, *Nat. Chem. Biol.*, 2022, **18**, 1319–1329.

188 G. Krainer, T. J. Welsh, J. A. Joseph, J. R. Espinosa, S. Wittmann, A. de Csilléry, A. Sridhar, Z. Toprakcioglu, G. Gudiškytė, M. A. Czekalska, W. E. Arter, J. Guillén-Boixet, T. M. Franzmann, S. Qamar, P. S. George-Hyslop, A. A. Hyman, R. Collepardo-Guevara, S. Alberti and T. P. J. Knowles, *Nat. Commun.*, 2021, **12**, 1085.

189 S. Park, R. Barnes, Y. Lin, B.-J. Jeon, S. Najafi, K. T. Delaney, G. H. Fredrickson, J.-E. Shea, D. S. Hwang and S. Han, *Commun. Chem.*, 2020, **3**, 83.

190 T. Lu, K. K. Nakashima and E. Spruijt, *J. Phys. Chem. B*, 2021, **125**, 3080–3091.

191 G. L. Dignon, W. Zheng, Y. C. Kim and J. Mittal, *ACS Cent. Sci.*, 2019, **5**, 821–830.

192 J. B. Otis and S. Sharpe, *Biomacromolecules*, 2022, **23**, 5225–5238.

193 K. M. Ruff, S. Roberts, A. Chilkoti and R. V. Pappu, *J. Mol. Biol.*, 2018, **430**, 4619–4635.

194 X. Zeng, C. Liu, M. J. Fossat, P. Ren, A. Chilkoti and R. V. Pappu, *APL Mater.*, 2021, **9**, 021119.

195 M. Dzuricky, B. A. Rogers, A. Shahid, P. S. Cremer and A. Chilkoti, *Nat. Chem.*, 2020, **12**, 814–825.

196 J. R. Simon, N. J. Carroll, M. Rubinstein, A. Chilkoti and G. P. López, *Nat. Chem.*, 2017, **9**, 509–515.

197 L. D. Muiznieks, S. Sharpe, R. Pomès and F. W. Keeley, *J. Mol. Biol.*, 2018, **430**, 4741–4753.

198 S. Roberts, M. Dzuricky and A. Chilkoti, *FEBS Lett.*, 2015, **589**, 2477–2486.

199 N. K. Dutta, M. Y. Truong, S. Mayavan, N. Roy Choudhury, C. M. Elvin, M. Kim, R. Knott, K. M. Nairn and A. J. Hill, *Angew. Chem., Int. Ed.*, 2011, **50**, 4428–4431.

200 K. Julius, J. Weine, M. Gao, J. Latarius, M. Elbers, M. Paulus, M. Tolan and R. Winter, *Macromolecules*, 2019, **52**, 1772–1784.

201 Y. Akahoshi, H. Sugai, M. Mimura, Y. Shinkai, R. Kurita, K. Shiraki and S. Tomita, *Biomacromolecules*, 2023, **24**, 704–713.

202 T. Kaur, I. Alshareedah, W. Wang, J. Ngo, M. M. Moosa and P. R. Banerjee, *Biomolecules*, 2019, **9**, 71.

203 O. Annunziata, N. Asherie, A. Lomakin, J. Pande, O. Ogun and G. B. Benedek, *Proc. Natl. Acad. Sci. U. S. A.*, 2002, **99**, 14165–14170.

204 P. Dogra, A. Joshi, A. Majumdar and S. Mukhopadhyay, *J. Am. Chem. Soc.*, 2019, **141**, 20380–20389.

205 E. G. P. Stender, S. Ray, R. K. Norrild, J. A. Larsen, D. Petersen, A. Farzadfard, C. Galvagnion, H. Jensen and A. K. Buell, *Nat. Commun.*, 2021, **12**, 7289.

206 D. Q. P. Reis, S. Pereira, A. P. Ramos, P. M. Pereira, L. Morgado, J. Calvário, A. O. Henriques, M. Serrano and A. S. Pina, *Nat. Commun.*, 2024, **15**, 9368.

207 M. Heidenreich, J. M. Georgeson, E. Locatelli, L. Rovigatti, S. K. Nandi, A. Steinberg, Y. Nadav, E. Shimoni, S. A. Safran, J. P. K. Doye and E. D. Levy, *Nat. Chem. Biol.*, 2020, **16**, 939–945.

208 S. C. Weber, *Curr. Opin. Cell Biol.*, 2017, **46**, 62–71.

209 H. Tao, C. Rigoni, H. Li, A. Koistinen, J. V. I. Timonen, J. Zhou, E. Kontturi, O. J. Rojas and G. Chu, *Nat. Commun.*, 2023, **14**, 5277.

210 L. S. Taylor and G. G. Z. Zhang, *Adv. Drug Delivery Rev.*, 2016, **101**, 122–142.

211 J. Chen, A. Tsuchida, A. D. Malay, K. Tsuchiya, H. Masunaga, Y. Tsuji, M. Kuzumoto, K. Urayama, H. Shintaku and K. Numata, *Nat. Commun.*, 2024, **15**, 527.

212 X. Gui, F. Luo, Y. Li, H. Zhou, Z. Qin, Z. Liu, J. Gu, M. Xie, K. Zhao, B. Dai, W. S. Shin, J. He, L. He, L. Jiang, M. Zhao, B. Sun, X. Li, C. Liu and D. Li, *Nat. Commun.*, 2019, **10**, 2006.

213 M. Linsenmeier, M. Hondele, F. Grigolato, E. Secchi, K. Weis and P. Arosio, *Nat. Commun.*, 2022, **13**, 3030.

214 A. Boija, I. A. Klein and R. A. Young, *Cancer Cell*, 2021, **39**, 174–192.

215 I. Alshareedah, W. M. Borcherds, S. R. Cohen, A. Singh, A. E. Posey, M. Farag, A. Bremer, G. W. Strout, D. T. Tomares, R. V. Pappu, T. Mittag and P. R. Banerjee, *Nat. Phys.*, 2024, **20**, 1482–1491.

216 L. Jawerth, E. Fischer-Friedrich, S. Saha, J. Wang, T. Franzmann, X. Zhang, J. Sachweh, M. Ruer, M. Ijavi, S. Saha, J. Mahamid, A. A. Hyman and F. Jülicher, *Science*, 2020, **370**, 1317–1323.

217 A. Abyzov, M. Blackledge and M. Zweckstetter, *Chem. Rev.*, 2022, **122**, 6719–6748.

218 Z. Monahan, V. H. Ryan, A. M. Janke, K. A. Burke, S. N. Rhoads, G. H. Zerze, R. O'Meally, G. L. Dignon, A. E. Conicella, W. Zheng, R. B. Best, R. N. Cole, J. Mittal, F. Shewmaker and N. L. Fawzi, *EMBO J.*, 2017, **36**, 2951–2967.

219 W. M. Aumiller and C. D. Keating, *Nat. Chem.*, 2016, **8**, 129–137.

220 F. Luo, X. Gui, H. Zhou, J. Gu, Y. Li, X. Liu, M. Zhao, D. Li, X. Li and C. Liu, *Nat. Struct. Mol. Biol.*, 2018, **25**, 341–346.

221 A. Garaizar, J. R. Espinosa, J. A. Joseph, G. Krainer, Y. Shen, T. P. J. Knowles and R. Collepardo-Guevara, *Proc. Natl. Acad. Sci. U. S. A.*, 2022, **119**, e2119800119.

222 R. Chang, C. Yuan, P. Zhou, R. Xing and X. Yan, *Acc. Chem. Res.*, 2024, **57**, 289–301.

223 C. Yuan, R. Xing, J. Cui, W. Fan, J. Li and X. Yan, *CCS Chem.*, 2024, **6**, 255–265.

224 P. Zhou, R. Xing, Q. Li, J. Li, C. Yuan and X. Yan, *Matter*, 2023, **6**, 1945–1963.

225 R. Dec, W. Dzwolak and R. Winter, *J. Am. Chem. Soc.*, 2024, **146**, 6045–6052.

226 A. Levin, T. A. Hakala, L. Schnaider, G. J. L. Bernardes, E. Gazit and T. P. J. Knowles, *Nat. Rev. Chem.*, 2020, **4**, 615–634.

227 C. Donau, F. Späth, M. Sosson, B. A. K. Kriebisch, F. Schnitter, M. Tena-Solsona, H.-S. Kang, E. Salibi, M. Sattler, H. Mutschler and J. Boekhoven, *Nat. Commun.*, 2020, **11**, 5167.

228 J. Ji, W. Wang and C. Chen, *Acta Biochim. Biophys. Sin.*, 2023, **55**, 1023–1033.

229 Y. Bao, H. Chen, Z. Xu, J. Gao, L. Jiang and J. Xia, *Angew. Chem., Int. Ed.*, 2023, **62**, e202307045.

230 E. M. Zhao, N. Suek, M. Z. Wilson, E. Dine, N. L. Pannucci, Z. Gitai, J. L. Avalos and J. E. Toettcher, *Nat. Chem. Biol.*, 2019, **15**, 589–597.

231 M. Mondal, P. E. Jankoski, L. D. Lee, D. M. Dinakarapandian, T.-Y. Chiu, W. S. Swetman, H. Wu, A. K. Paravastu, T. D. Clemons and V. Rangachari, *J. Am. Chem. Soc.*, 2024, **146**, 25299–25311.

232 L. Jia, S. Gao and Y. Qiao, *Small Methods*, 2024, **8**, 2301724.

233 N. Schneider, F.-G. Wieland, D. Kong, A. A. M. Fischer, M. Hörner, J. Timmer, H. Ye and W. Weber, *Sci. Adv.*, 2021, **7**, eabd3568.

234 Y. Shin, J. Berry, N. Pannucci, M. P. Haataja, J. E. Toettcher and C. P. Brangwynne, *Cell*, 2017, **168**, 159–171.

235 E. H. Brumbaugh-Reed, Y. Gao, K. Aoki and J. E. Toettcher, *Nat. Commun.*, 2024, **15**, 6717.

236 N. Martin, L. Tian, D. Spencer, A. Coutable-Pennarun, J. L. R. Anderson and S. Mann, *Angew. Chem., Int. Ed.*, 2019, **58**, 14594–14598.

237 N. Ikeuchi, T. Komachi, K. Murayama, H. Asanuma, A. Maruyama and N. Shimada, *ACS Appl. Mater. Interfaces*, 2021, **13**, 5652–5659.

238 M. Abbas, W. P. Lipiński, K. K. Nakashima, W. T. S. Huck and E. Spruijt, *Nat. Chem.*, 2021, **13**, 1046–1054.

239 Y. Sun, X. Xu, L. Chen, W. L. Chew, Y. Ping and A. Miserez, *ACS Nano*, 2023, **17**, 16597–16606.

240 Y. Dai, C. F. Chamberlayne, M. S. Messina, C. J. Chang, R. N. Zare, L. You and A. Chilkoti, *Chem*, 2023, **9**, 1594–1609.

241 X. Wang, J. Liu, C. Mao and Y. Mao, *Cell Commun. Signaling*, 2024, **22**, 143.

242 K. Guo, J. Zhang, P. Huang, Y. Xu, W. Pan, K. Li, L. Chen, L. Luo, W. Yu, S. Chen, S. He, Z. Wei and C. Yu, *Cell Rep.*, 2023, **42**, 113321.

243 S. Yang, C. Liu, Y. Guo, G. Li, D. Li, X. Yan and X. Zhu, *Proc. Natl. Acad. Sci. U. S. A.*, 2022, **119**, e2122420119.

244 S. Yang, Y. Yu, S. Jo, Y. Lee, S. Son and K. H. Lee, *Nat. Commun.*, 2024, **15**, 10394.

245 R. Niwayama, H. Nagao, T. S. Kitajima, L. Hufnagel, K. Shinohara, T. Higuchi, T. Ishikawa and A. Kimura, *PLoS One*, 2016, **11**, e0159917.

246 A. Brown, *Nat. Rev. Mol. Cell Biol.*, 2000, **1**, 153–156.

247 M. J. Harrington, R. Mezzenga and A. Miserez, *Nat. Rev. Bioeng.*, 2024, **2**, 260–278.

248 Y. Song, *Biomater. Sci.*, 2024, **12**, 1943–1949.

249 J. Liu, F. Zhorabek and Y. Chau, *Matter*, 2022, **5**, 2787–2812.

250 G. C. Yeo, B. Aghaei-Ghareh-Bolagh, E. P. Brackenreg, M. A. Hiob, P. Lee and A. S. Weiss, *Adv. Healthcare Mater.*, 2015, **4**, 2530–2556.

251 A. K. Varanko, J. C. Su and A. Chilkoti, *Annu. Rev. Biomed. Eng.*, 2020, **22**, 343–369.

252 A. Huang and L. Su, *Acc. Mater. Res.*, 2023, **4**, 729–732.

253 H. J. Kim, B. H. Hwang, S. Lim, B.-H. Choi, S. H. Kang and H. J. Cha, *Biomaterials*, 2015, **72**, 104–111.

254 E. Y. Jeon, S.-H. Um, J. Park, Y. Jung, C.-H. Cheon, H. Jeon and J. J. Chung, *Small*, 2022, **18**, 2200416.

255 M. Cui, X. Wang, B. An, C. Zhang, X. Gui, K. Li, Y. Li, P. Ge, J. Zhang, C. Liu and C. Zhong, *Sci. Adv.*, 2019, **5**, eaax3155.

256 W. H. Park, J. Lee, H. J. Kim, K. I. Joo and H. J. Cha, *Chem. Eng. J.*, 2022, **446**, 137272.

257 H. J. Kim, B.-H. Choi, S. H. Jun and H. J. Cha, *Adv. Healthcare Mater.*, 2016, **5**, 3191–3202.

258 Y. Sun, S. Y. Lau, Z. W. Lim, S. C. Chang, F. Ghadessy, A. Partridge and A. Miserez, *Nat. Chem.*, 2022, **14**, 274–283.

259 L. Jiang, Y. Zeng, H. Li, Z. Lin, H. Liu, J. J. Richardson, Z. Gao, D. Wu, L. Liu, F. Caruso and J. Zhou, *J. Am. Chem. Soc.*, 2023, **145**, 24108–24115.

260 C. Dong and Y. Lv, *Polymers*, 2016, **8**, 42.

261 Y. Sun, S. H. Hiew and A. Miserez, *Acc. Chem. Res.*, 2024, **57**, 164–174.

262 S. Acosta, L. Quintanilla-Sierra, L. Mbundi, V. Reboto and J. C. Rodríguez-Cabello, *Adv. Funct. Mater.*, 2020, **30**, 1909050.

263 S. Chen, Q. Guo and J. Yu, *Aggregate*, 2022, **3**, e293.

264 F. Jehle, E. Macías-Sánchez, S. Sviben, P. Fratzl, L. Bertinetti and M. J. Harrington, *Nat. Commun.*, 2020, **11**, 862.

265 B. Wu, P. Ding, M. Wang, M. A. Cohen Stuart and J. Wang, *Matter*, 2023, **6**, 2517–2519.

266 J. Liu, E. Spruijt, A. Miserez and R. Langer, *Nat. Rev. Mater.*, 2023, **8**, 139–141.

267 D. M. Mitrea, M. Mittasch, B. F. Gomes, I. A. Klein and M. A. Murcko, *Nat. Rev. Drug Discovery*, 2022, **21**, 841–862.

268 M. J. Mitchell, M. M. Billingsley, R. M. Haley, M. E. Wechsler, N. A. Peppas and R. Langer, *Nat. Rev. Drug Discovery*, 2021, **20**, 101–124.

269 A. M. Vargason, A. C. Anselmo and S. Mitragotri, *Nat. Biomed. Eng.*, 2021, **5**, 951–967.

270 X. Zhu, J. Yuan, R. Chang, W. Fan, Y. Wang, H. Li, Y. Zhang, P. Zhou and X. Yan, *Colloids Surf., A*, 2024, **697**, 134331.

271 R. Tenchov, R. Bird, A. E. Curtze and Q. Zhou, *ACS Nano*, 2021, **15**, 16982–17015.

272 N. R. Johnson and Y. Wang, *Expert Opin. Drug Delivery*, 2014, **11**, 1829–1832.

273 C. Forenzo and J. Larsen, *Mol. Pharmaceutics*, 2023, **20**, 4387–4403.

274 Y. Tian, Q. Hu, Z. Sun, Y. Yu, X. Li, T. Tian, X. Bi, Y. Li, B. Niu and Z. Zhang, *Small*, 2024, **20**, 2311890.

275 Z. W. Lim, V. B. Varma, R. V. Ramanujan and A. Miserez, *Acta Biomater.*, 2020, **110**, 221–230.

276 S. Yu, W. Chen, G. Liu, B. Flores, E. L. DeWolf, B. Fan, Y. Xiang and M. J. Webber, *J. Am. Chem. Soc.*, 2024, **146**, 7498–7505.

277 J. Liu, R. Feng and Y. Chau, *Matter*, 2022, **5**, 1637–1639.

278 A. Shebanova, Q. M. Perrin, K. Zhu, S. Gudlur, Z. Chen, Y. Sun, C. Huang, Z. W. Lim, E. A. Mondarte, R. Sun, S. Lim, J. Yu, Y. Miao, A. N. Parikh, A. Ludwig and A. Miserez, *Adv. Sci.*, 2024, **11**, 2402652.

279 H.-X. Zhou, D. Kota, S. Qin and R. Prasad, *Chem. Rev.*, 2024, **124**, 8550–8595.

280 K. K. Nakashima, M. H. I. van Haren, A. A. M. André, I. Robu and E. Spruijt, *Nat. Commun.*, 2021, **12**, 3819.

281 A. Ianeselli, D. Tetiker, J. Stein, A. Kühnlein, C. B. Mast, D. Braun and T. Y. Dora Tang, *Nat. Chem.*, 2022, **14**, 32–39.

282 A. F. Mason, B. C. Buddingh, D. S. Williams and J. C. M. van Hest, *J. Am. Chem. Soc.*, 2017, **139**, 17309–17312.

283 F. Pir Cakmak, A. M. Marianelli and C. D. Keating, *Langmuir*, 2021, **37**, 10366–10375.

284 Y. Ji, Y. Lin and Y. Qiao, *J. Am. Chem. Soc.*, 2023, **145**, 12576–12585.

285 M. Abbas, J. O. Law, S. N. Grellscheid, W. T. S. Huck and E. Spruijt, *Adv. Mater.*, 2022, **34**, 2202913.

286 A. Agrawal, J. F. Douglas, M. Tirrell and A. Karim, *Proc. Natl. Acad. Sci. U. S. A.*, 2022, **119**, e2203483119.

287 A. Agrawal, A. Radakovic, A. Vonteddu, S. Rizvi, V. N. Huynh, J. F. Douglas, M. V. Tirrell, A. Karim and J. W. Szostak, *Sci. Adv.*, 2024, **10**, eadn9657.

288 U. Pramanik, A. Das, E. M. Brown, H. L. Struckman, H. Wang, S. Stealey, M. L. Sprunger, A. Wasim, J. Fascetti, J. Mondal, J. R. Silva, S. P. Zustiak, M. E. Jackrel and J. S. Rudra, *bioRxiv*, 2024, DOI: 10.1101/2024.09.10.612317.

289 B. C. Buddingh and J. C. M. van Hest, *Acc. Chem. Res.*, 2017, **50**, 769–777.

290 A. J. Dzieciol and S. Mann, *Chem. Soc. Rev.*, 2012, **41**, 79–85.

291 Z. Lin, T. Beneyton, J.-C. Baret and N. Martin, *Small Methods*, 2023, **7**, 2300496.

292 H. Wu and Y. Qiao, *Supramol. Mater.*, 2022, **1**, 100019.

293 W. Mu, L. Jia, M. Zhou, J. Wu, Y. Lin, S. Mann and Y. Qiao, *Nat. Chem.*, 2024, **16**, 158–167.

294 W. Mu, Z. Ji, M. Zhou, J. Wu, Y. Lin and Y. Qiao, *Sci. Adv.*, 2021, **7**, eabf9000.

295 N. A. Yewdall, A. A. M. André, T. Lu and E. Spruijt, *Curr. Opin. Colloid Interface Sci.*, 2021, **52**, 101416.

296 N. Martin, *ChemBioChem*, 2019, **20**, 2553–2568.

297 C. D. Crowe and C. D. Keating, *Interface Focus*, 2018, **8**, 20180032.

298 E. Sokolova, E. Spruijt, M. M. K. Hansen, E. Dubuc, J. Groen, V. Chokkalingam, A. Piruska, H. A. Heus and W. T. S. Huck, *Proc. Natl. Acad. Sci. U. S. A.*, 2013, **110**, 11692–11697.

299 J. Liu, F. Zhorabek, X. Dai, J. Huang and Y. Chau, *ACS Cent. Sci.*, 2022, **8**, 493–500.

300 M. Seal, O. Weil-Ktorza, D. Despotović, D. S. Tawfik, Y. Levy, N. Metanis, L. M. Longo and D. Goldfarb, *J. Am. Chem. Soc.*, 2022, **144**, 14150–14160.

301 T. Y. Dora Tang, C. Rohaida Che Hak, A. J. Thompson, M. K. Kuimova, D. S. Williams, A. W. Perriman and S. Mann, *Nat. Chem.*, 2014, **6**, 527–533.

302 N. Gao, C. Xu, Z. Yin, M. Li and S. Mann, *J. Am. Chem. Soc.*, 2022, **144**, 3855–3862.

303 T. Lu, S. Javed, C. Bonfio and E. Spruijt, *Small Methods*, 2023, **7**, 2300294.

304 C. D. Reinkemeier and E. A. Lemke, *Curr. Opin. Chem. Biol.*, 2021, **64**, 174–181.

305 S. Lim and D. S. Clark, *Trends Biotechnol.*, 2024, **42**, 496–509.

306 I. B. A. Smokers, B. S. Visser, A. D. Slootbeek, W. T. S. Huck and E. Spruijt, *Acc. Chem. Res.*, 2024, **57**, 1885–1895.

307 T. J. Nott, T. D. Craggs and A. J. Baldwin, *Nat. Chem.*, 2016, **8**, 569–575.

308 A. B. Cook, S. Novosedlik and J. C. M. van Hest, *Acc. Mater. Res.*, 2023, **4**, 287–298.

309 L. L. J. Schoenmakers, N. A. Yewdall, T. Lu, A. A. M. André, F. H. T. Nelissen, E. Spruijt and W. T. S. Huck, *ACS Synth. Biol.*, 2023, **12**, 2004–2014.

310 K. K. Nakashima, J. F. Baaij and E. Spruijt, *Soft Matter*, 2018, **14**, 361–367.

311 E. Dine, A. A. Gil, G. Uribe, C. P. Brangwynne and J. E. Toettcher, *Cell Systems*, 2018, **6**, 655–663.

312 M. Matsuo and K. Kurihara, *Nat. Commun.*, 2021, **12**, 5487.

313 A. O. Robinson, J. Lee, A. Cameron, C. D. Keating and K. P. Adamala, *ACS Biomater. Sci. Eng.*, 2024, **10**, 773–781.

314 C. M. Green, D. Sementa, D. Mathur, J. S. Melinger, P. Deshpande, S. Elbaum-Garfinkle, I. L. Medintz, R. V. Ulijn and S. A. Díaz, *Commun. Chem.*, 2024, 7, 49.

315 T. Y. Dora Tang, D. van Swaay, A. deMello, J. L. Ross Anderson and S. Mann, *Chem. Commun.*, 2015, **51**, 11429–11432.

316 R. Xing, C. Yuan, W. Fan, X. Ren and X. Yan, *Sci. Adv.*, 2023, **9**, eadd8105.

317 S. Cao, W. Fan, R. Chang, C. Yuan and X. Yan, *CCS Chem.*, 2024, **6**, 2814–2824.

318 C. Yuan, W. Fan, P. Zhou, R. Xing, S. Cao and X. Yan, *Nat. Nanotechnol.*, 2024, **19**, 1840–1848.